New Phytologist

Research

Single-cell RNA-sequencing of *Nicotiana attenuata* corolla cells reveals the biosynthetic pathway of a floral scent

Moonyoung Kang, Yuri Choi, Hyeonjin Kim and Sang-Gyu Kim

Department of Biological Sciences, Korea Advanced Institute for Science and Technology, Daejeon 34141, Korea

Author for correspondence:
Sang-Gyu Kim
Email: sgkim1@kaist.ac.kr

Received: *13 September 2021*
Accepted: *5 January 2022*

New Phytologist (2022) **234:** 527–544
doi: 10.1111/nph.17992

Key words: 10x genomics, benzylacetone, corolla, floral scents, *Nicotiana attenuata*, scRNA-Seq.

Summary

- High-throughput single-cell RNA sequencing (scRNA-Seq) identifies distinct cell populations based on cell-to-cell heterogeneity in gene expression. By examining the distribution of the density of gene expression profiles, we can observe the metabolic features of each cell population.
- Here, we employ the scRNA-Seq technique to reveal the entire biosynthetic pathway of a flower volatile.
- The corolla of the wild tobacco *Nicotiana attenuata* emits a bouquet of scents that are composed mainly of benzylacetone (BA). Protoplasts from the *N. attenuata* corolla limbs and throat cups were isolated at three different time points, and the transcript levels of > 16 000 genes were analyzed in 3756 single cells.
- We performed unsupervised clustering analysis to determine which cell clusters were involved in BA biosynthesis. The biosynthetic pathway of BA was uncovered by analyzing gene co-expression in scRNA-Seq datasets and by silencing candidate genes in the corolla.
- In conclusion, the high-resolution spatiotemporal atlas of gene expression provided by scRNA-Seq reveals the molecular features underlying cell-type-specific metabolism in a plant.

Introduction

Flowers produce diverse volatiles for various ecological interactions. More than 1700 different floral scents have been identified (Knudsen *et al.*, 2006): these scents are classified as terpenoids, fatty acid-derivatives, and phenylpropanoid/benzenoids, according to their biosynthetic pathways (Muhlemann *et al.*, 2014; Knudsen & Gershenzon, 2020). One molecular mechanism underlying floral scent diversity is the duplication followed by subsequent mutation (neofunctionalization) of biosynthetic genes (Baudino *et al.*, 2020). A mutation in a coding region can generate new volatile compounds by binding to the original substrate or to similar substrates. For example, a single amino-acid substitution in *Oryza sativa* terpene synthase 1 (TPS1) changes the ratio between two products: (*E*)-β-caryophyllene and germacrene A (Chen *et al.*, 2014). In addition, a single amino-acid substitution in salicylic acid methyltransferase isolated from *Datura wrightii* (Barkman *et al.*, 2007) and in *O*-methyltransferase isolated from *Thalictrum tuberosum* (Frick & Kutchan, 1999) alters a binding affinity to substrates, which results in different products. Mutations in a *cis*-regulatory element may trigger changes in the spatiotemporal expression of biosynthetic enzymes, resulting in the generation of a new metabolic pathway. Because small changes in enzymes can produce new compounds, identifying the genes responsible for floral scent biosynthesis requires a multidisciplinary approach that includes functional prediction based on sequence homology to characterized enzymes, biochemical assay, and *in vivo* gene manipulation.

To identify the genes responsible for floral scent production, DNA/RNA sequencing techniques, microarrays, and several statistical methods have been widely used. Candidate genes have been prioritized by investigating correlations among transcript abundances and target compounds (Verdonk *et al.*, 2005; Magnard *et al.*, 2015; Xu *et al.*, 2018). By analyzing differential gene expression among the rose cultivars that vary widely in floral scent emission, researchers identified a sesquiterpene synthase (Guterman *et al.*, 2002) and a nudix hydrolase (Magnard *et al.*, 2015), a new type of monoterpene synthase. In addition, when a biosynthetic gene in a multi-step pathway is available, this gene can be used as 'bait' to calculate its degree of association to the entire transcriptome (gene co-expression network analysis) (Wisecaver *et al.*, 2017), and a gene cluster that regulates the production of metabolites can be constructed (Li *et al.*, 2020). For instance, TPS11 enzyme in *Arabidopsis thaliana* flowers synthesizes (+)-α-barbatene and (+)-thujopsene. These volatiles are further oxidized by CYP706A3, which was discovered through co-expression analysis with TPS11 (Boachon *et al.*, 2019). These successful identification of biosynthetic genes of specialized volatiles through gene-to-metabolite or gene-to-gene correlation requires genetic, environmental, tissue-specific diversity in the material analyzed (Wong *et al.*, 2020).

Flower scents are mainly synthesized in the petals. In particular, several volatile biosynthetic genes are detected in the

epidermal cells of petals, for example, (*S*)-linalool synthase (Dudareva *et al.*, 1996) and isoeugenol *O*-methyltransferase (Dudareva & Pichersky, 2000) in *Clarkia breweri* flowers; benzoic acid carboxyl methyltransferase in *Antirrhinum majus* flowers (Kolosova *et al.*, 2001); and orcinol *O*-methyltransferase in rose cultivars (Scalliet *et al.*, 2006). Separating scent-producing cells from the rest of the cells in the entire petals can increase the accuracy of a co-expression analysis: laser microdissection procedures and marker-based cell sorting methods have been used to isolate cells (Libault *et al.*, 2017; Wong *et al.*, 2020). Recently, several high-throughput single-cell RNA sequencing (scRNA-Seq) techniques have emerged for analyzing transcriptomes expressed in single cells isolated from tissues or organs. The scRNA-Seq database shows cellular heterogeneity and molecular processes specific to cell types in plant tissues, such as roots (Denyer *et al.*, 2019; Jean-Baptiste *et al.*, 2019; Ryu *et al.*, 2019; Shulse *et al.*, 2019), leaves (Lopez-anido *et al.*, 2020; Kim *et al.*, 2021), and shoot apical meristems (Satterlee *et al.*, 2020; Zhang *et al.*, 2021). Assuming that all biosynthetic genes of a given floral scent are expressed in a single cell and that the regulation of those genes is coordinated, the scRNA-Seq database of petals can be useful in prioritizing candidate genes, as it allows researchers to calculate correlations among genes expressed in several thousands of petal cells (Wong *et al.*, 2020).

Flowers in the wild tobacco *Nicotiana attenuata* emit benzylacetone (BA, 4-phenyl-2-butanone) at night to attract pollinators, such as *Manduca sexta* hawkmoths (Euler & Baldwin, 1996; Baldwin, 1997; Haverkamp *et al.*, 2016), and to prevent floral damage from cucumber beetles (Kessler *et al.*, 2019). Most BA is produced from corolla limbs (Euler & Baldwin, 1996; Kessler & Baldwin, 2007), and is regulated by the circadian clock (Yon *et al.*, 2016). L-Phenylalanine (Phe) is a precursor of BA, and *N. attenuata* phenylalanine ammonia-lyase 4 (NaPAL4) is known to be the first enzyme in the BA biosynthetic pathway (Guo *et al.*, 2020). In addition, the co-silencing of polyketide synthase 2/3 (NaPKS2/3, previously NaCHAL2/3) reduced the level of BA emission (Kessler *et al.*, 2008; Guo *et al.*, 2020), which suggested that one or more NaPKSs catalyze a condensation reaction with malonyl-Coenzyme A (CoA) to produce BA intermediates, as shown in an ornamental rhubarb (*Rheum palmatum*, Abe *et al.*, 2001). In the plant kingdom, the major Phe-derived floral volatiles are phenylpropanoid (a phenyl ring with a three-carbon side chain, C_6–C_3) and benzenoid (C_6–C_1) (Widhalm & Dudareva, 2015), whose biosyntheses are generally initiated by PAL and two types of CoA ligases (4-coumarate-CoA ligase, 4CL; cinnamate-CoA ligase, CNL) (Klempien *et al.*, 2012; Qualley *et al.*, 2012). However, BA possesses a C_6–C_4 structure (phenylbutanoids). To identify the entire biosynthetic pathway of this rare floral scent (Knudsen *et al.*, 2006), we performed the scRNA-Seq of protoplasts isolated from the *N. attenuata* corolla limbs and throat cups, and defined distinct cell clusters based on the cell-to-cell variation in gene expression. Gene co-expression analysis with scRNA-Seq datasets and *in vivo* and *in vitro* characterization of enzyme activity enable us to identify the entire set of BA biosynthetic genes.

Materials and Methods

Plant materials and protoplasting

Seeds of *N. attenuata* Utah 39th inbred line originating from a natural population in Utah were germinated on Petri dishes with Gamborg's B5 medium including vitamins (Duchefa Biochemie, Haarlem, the Netherlands), as described previously (Krügel *et al.*, 2002). The original collection of the seeds was done on private lands and no specific permissions for seed collections were necessary. Plants were grown under 16 h : 8 h, light : dark conditions at 26°C with ±2°C variation. Protoplasts were isolated from approximately 40 corolla limbs and throat cups of *N. attenuata* at Zeitgeber Time 8 (ZT 8, 8 h after the onset of light), ZT 12, and ZT 16 of the first day of flower opening. Corolla limbs and throat cups were excised by scalpel and immediately immersed in a plant culture dish containing 25 ml of cell-wall-degrading enzyme mixtures (1.5% (w/v) cellulase R-10; Yakult, Tokyo, Japan; 0.4% (w/v) macerozyme R-10, Yakult; 9% (w/v) mannitol, Duchefa Biochemie; 0.1% (w/v) 2-(*N*-morpholino)ethanesulfonic acid (MES), Duchefa Biochemie; 0.1% bovine serum albumin (BSA), Sigma-Aldrich, St Louis, MO, USA) (Yoo *et al.*, 2007). After 5 min of vacuum treatment, tissues were shaken at 20 rpm on an orbital shaker for 30 min in the dark, and the cell suspension was filtered onto a Petri dish using a 40 μm cell strainer (Corning, NY, USA). The protoplast suspensions were centrifuged at 100 ***g*** for 5 min, and the resulting pellets were resuspended and washed with 10% (w/v) mannitol solution. Cells were washed, centrifuged again, and finally filtered with 40 μm Flowmi tip strainer (Bel-Art SP Scienceware; Wayne, NJ, USA). Cell concentration and viability were calculated using 0.2% trypan blue on Cellometer Auto 2000 (Nexcelom Bioscience, Lawrence, MA, USA). All samples showed a viability over 70%. The entire protoplasting procedure was completed in 2 h.

Generation of single-cell RNA sequencing library and feature-barcode matrices

Cell suspensions were loaded into the 10x Genomics Chromium single-cell microfluidics device with the Single Cell 3′ Library & Gel Bead Kit v.3 (10x Genomics, leasanton, CA, USA) according to the manufacturer's instructions. Twelve PCR cycles were used for complementary DNA (cDNA) amplification, and 14 to 15 PCR cycles were performed for ligating adaptors. The library quality and size were checked using DNA high-sensitivity D5000 ScreenTape System (Agilent Technologies, Santa Clara, CA, USA). The single-cell RNA sequencing (scRNA-Seq) libraries were sequenced on the HiSeq X Ten platform (Illumina, San Diego, CA, USA) at Macrogen (Seoul, Republic of Korea). Approximately 400 000 reads and 1300 genes were detected per cell. Total 19 553, 19 842, and 18 917 genes were detected from ZT 8, ZT 12, and ZT 16 datasets, respectively.

Sequencing data were demultiplexed with mkfastq command in Cell Ranger (v.3.1.0) (10x Genomics) to generate fastq files. Expression matrices were also generated through the Cell Ranger pipeline, by aligning reads to the *N. attenuata* genome

(NIATTr2). The Cellranger mkref command was used after filtering the GTF file to include only protein-coding genes in the *N. attenuata* genome. Feature-barcode matrix was generated after preprocessing, aligning, counting UMI, and filtering cells using Cell Ranger count command with default options.

Single-cell expression matrices were row-summed to generate pseudo-bulk datasets from scRNA-Seq datasets. Conventional bulk RNA sequencing (bulk RNA-Seq) was performed with corolla limbs at three different time points: ZT 8, ZT 12, and ZT 16. Pearson's correlation coefficient was calculated between these pseudo-bulk datasets and conventional bulk RNA-Seq datasets. Some of the stress-related genes were highly upregulated in three scRNA-Seq datasets ($\log_2$ fold change (FC) > 5); these genes (described in Supporting Information Table S1) were excluded from downstream analysis.

Uniform manifold approximation and projection visualization and marker gene identification

After filtering matrices, the SEURAT R package (v.3.2.0) was used for dimension reduction and visualization (Satija *et al.*, 2015; Butler *et al.*, 2018). Cells that expressed < 200 genes were discarded. To integrate the single-cell libraries generated from three different time points, the datasets were normalized separately by sctransform (SCT) (Hafemeister & Satija, 2019), and all features were selected for downstream integration. Pearson residuals were calculated by running PrepSCTIntegration, and anchors were identified by SCT normalization. Principal component analysis was conducted on the integrated dataset. Based on the top 50 principal components, distinct cell populations were defined by unsupervised clustering analysis (0.4 resolution) and visualized by uniform manifold approximation and projection (UMAP).

Marker genes of each cluster through all time points were selected by Wilcoxon rank sum test in Seurat's FindConservedMarkers function. Genes over 0.25 log-FC relative to other clusters and Bonferroni-corrected *P*-value < 0.05 were chosen as upregulated genes in individual clusters. Average levels of transcripts and percentages of cells expressing the marker per cluster were visualized by color and size in dot plots or in violin plots. Based on the predicted functions of marker genes, we characterized clusters as epidermis, parenchyma, chlorenchyma, pollen, and vasculatures.

Gene co-expression analysis

Twenty bulk RNA-Seq datasets containing 14 tissue types from *N. attenuata* were downloaded from the sequence read archive database (Li *et al.*, 2016). TPM values of each gene were used for calculating Spearman's correlation coefficients between genes, and coefficients of each gene with *N. attenuata PAL4* (A4A49_25502) were extracted and visualized as histograms. For scRNA-Seq co-expression analysis, unique molecular identifier (UMI) values of genes were divided by the sum of UMI in each cell and multiplied by 100 000 to normalize the values. The normalized UMIs of each gene were used for calculating Spearman's correlation coefficients between genes.

Genes with at least one UMI were assigned a value of 1, and others with no UMIs were assigned a value of 0. Cells with the value 1 of target gene were regarded as the cells expressing the gene. This binary matrix was then used as an input for an UpSet plot. The UpSet plot was drawn in COMPLEXUPSET package (v.0.7.3) (Lex *et al.*, 2014; Krassowski, 2020). For visualizing the cells that express four BA biosynthetic genes, the FeaturePlot function in the SEURAT package was used with the parameters: min.cutoff = 'q10', max.cutoff = 'q90', and blend = T.

Virus-induced gene silencing

To silence a target gene in *N. attenuata* corolla, virus-induced gene silencing (VIGS) using tobacco rattle virus (TRV)-based vectors was performed (Saedler & Baldwin, 2004). A 250 bp fragment of the gene of interest was designed using the SGN VIGS Tool (Fernandez-Pozo *et al.*, 2015) and cloned into the TRV2 vector. The *Agrobacterium tumefaciens* AGL1 strain harboring the TRV2 target gene was mixed with *Agrobacterium* containing TRV1 just before infiltration. About 1 to 2 ml of *Agrobacterium* solution was injected into *N. attenuata* rosette leaves (three leaves per plant). The infiltrated plants were incubated in the dark at 22°C for 2 d and then acclimated under weak light conditions in a growth chamber for 2 d. Later, the infiltrated plants were grown under 16 h : 8 h, light : dark conditions at 26°C with ±2°C variation. TRV2-eGFP was used as a negative control, and phytoene desaturase (PDS) gene was silenced (TRV2-PDS) in parallel to check whether VIGS works in flowers for each experimental condition. We measured the level of BA and BA-biosynthetic genes in flowers from virus-infected plants once TRV2-PDS flowers produced white flowers. The silencing efficiency of individual corolla was measured by quantitative reverse transcription polymerase chain reaction (qRT-PCR). Total RNA was extracted using RNeasy Plant Mini Kit (Qiagen, Hilden, Germany), and genomic DNA was removed by treating RNase-free DNase I (Qiagen). Extracted RNA was reverse-transcribed using oligo dT and SuperScript™ IV reverse transcriptase (Thermo Fisher Scientific, Waltham, MA, USA) following manufacturer's protocols. Quantitative RT-PCR was performed on AriaMx real-time PCR System (Agilent Technologies) with TB Green Premix EX Taq (Takara, Shiga, Japan). Transcript levels were quantified by the comparative C_T method (Schmittgen & Livak, 2008). The C_q values were normalized to the value of the internal control gene, *NaEF1a* (elongation factor 1a, ΔC_q). To calculate individual FC values, each biological replicate sample (ΔC_q) was normalized by one calibrator sample in the TRV2-GFP control group ($\Delta\Delta C_q$) and presented as points in graph. Primers used in this study are listed in Table S2.

Headspace and internal volatile sampling and gas chromatography–mass spectrometry (GC–MS) analysis

Flower headspace volatiles were trapped in silicone tubing (ST) and analyzed as previously described (Kallenbach *et al.*, 2014). Briefly, before flowers start to open, a flower was excised and enclosed in a clean 8 ml glass vial with 300 µl of ultrapure water.

Clean ST, 1 cm in length, was placed directly over the corolla limb for 3 h (ZT 14–ZT 17), when the BA emission peaked (Yon *et al.*, 2016) and our last sampling for scRNA-Seq (ZT 16) was done. GCMS-QP2020 (Shimadzu, Kyoto, Japan) connected with a TD-30 thermal desorption unit (Shimadzu) was used for gas analysis. All standard compounds used in this study were purchased from Sigma-Aldrich.

For internal volatile sampling, 50 mg of corolla limbs and throat cups was finely ground in liquid nitrogen and resuspended in 1 ml of saturated calcium chloride solution spiked with tetralin as an internal standard (Joo *et al.*, 2019). A 1 cm length of clean ST was incubated in the resuspension solution overnight and shaken at 80 rpm. Incubated STs were rinsed with ultrapure water and dried under a gentle nitrogen flow. Room temperature-equilibrated STs were analyzed in GCMS-QP2020 connected with a TD-30 thermal desorption unit (Shimadzu).

Functional evaluation of benzylacetone biosynthetic enzymes

Codon-optimized BA biosynthetic gene sequences (Bioneer, Daejeon, Korea) or native coding sequences (CDSs) were cloned into a pET50 vector. *Escherichia coli* Rosetta (DE3) cells were transformed with pET50-a target gene and grown in LB broth media containing 50 μg ml^{-1} of kanamycin and 30 μg ml^{-1} of chloramphenicol at 37°C. When the optical density measured at 600 nm (OD_{600}) reached 0.5–0.6, protein expression was induced by adding 0.35 mM of isopropyl β-D-1-thiogalactopyranoside (IPTG). After incubating an additional 18–20 h at 18°C, cells were harvested and lysed in cell resuspension buffer supplemented with 0.5 mM phenylmethylsulfonyl fluoride (PMSF) by sonication. Cell resuspension buffers for each protein were prepared as previously described (Abe *et al.*, 2001; Koeduka *et al.*, 2011; Klempien *et al.*, 2012); for purifying recombinant proteins, soluble protein fractions were obtained by centrifugation at 16 200 ***g*** for 20 min at 4°C and loaded onto Ni-NTA agarose resin (Thermo Fisher Scientific), following manufacturer's instructions. The size and purity of eluted proteins were confirmed by Coomassie staining. To get rid of excess imidazole, proteins were dialyzed against the final dissolving buffers and then stored at −80°C.

The CoA ligase activity of Na4CL1 with *t*-cinnamic acid (Sigma-Aldrich) and its derivatives (4-coumaric acid, caffeic acid and ferulic acid; Sigma-Aldrich) was determined spectrophotometrically, as previously described (Klempien *et al.*, 2012). Briefly, the spectrophotometric assay was performed by monitoring the increase in absorption maximum on a microplate reader (311, 333, 346, and 345 nm for cinnamoyl-, coumaroyl-, caffeoyl-, and feruloyl-CoA, respectively). The assay reaction was performed with 250 μl solution containing 1.76 μg of purified Na4CL1 protein in 50 mM Tris/K phosphate/Na citrate pH 8.5, 2.5 mM adenosine triphosphate (ATP), 5 mM magnesium chloride ($MgCl_2$), 0.4 mM CoA, and various concentration of *t*-cinnamic acid and its derivatives. Reactions were started by adding substrates to each well. The extinction coefficient used for calculating cinnamoyl-CoA formation was 22 000 ml $mmol^{-1}$ cm^{-1} (Lee *et al.*, 1997); likewise, 21 000 ml $mmol^{-1}$ cm^{-1} for coumaroyl-CoA, 18 000 ml $mmol^{-1}$ cm^{-1} for caffeoyl-CoA, and 19 000 ml $mmol^{-1}$ cm^{-1} for feruloyl-CoA were used as extinction coefficients.

We purified NaPKS2 and NaPKS3 proteins as described previously (Abe *et al.*, 2001) and mixed NaPKS2 or NaPKS3 with the products formed during Na4CL1 spectrophotometric assays and malonyl-CoA. The reaction mixture contained 50 μl of Na4CL1 products (intended to contain final 40 μM of cinnamoyl-CoA in 500 μl reaction mixture), 40 μM malonyl-CoA, and 10 μg of NaPKS2 or NaPKS3 in a final volume of 500 μl of 100 mM potassium phosphate buffer containing 1 mM ethylenediaminetetraacetic acid (EDTA, pH 8.0). Mixtures were incubated at 30°C for 2 h, and reactions were stopped by adding 50 μl of glacial acetic acid. The products were immediately extracted with 1 ml of ethyl acetate via vigorous vortexing, and the ethyl acetate layer was concentrated using a freeze-dryer. All products were injected for gas chromatography–mass spectrometry (GC-MS) via a thermal desorption unit (Shimadzu).

Reducing activity of NaAER1 was determined spectrophotometrically, with modified reaction conditions as previously described (Koeduka *et al.*, 2011). The assay mixture contained 5 μg of purified NaAER1 proteins, 0.5 mM NADPH, and putative substrates (benzalacetone and vanillylidenacetone from Sigma-Aldrich; 4-hydroxy-benzalacetone from AA Blocks, San Diego, CA, USA) in different concentrations in final 200 μl of 125 mM MES-KOH (pH 7.5) buffer. Reactions were started by adding substrates. Decreasing absorbance at 340 nm for benzalacetone and 370 nm for 4-hydroxy-benzalacetone and vanillylidenacetone was monitored with the plate reader (Infinite M Nano; Tecan, Männedorf, Switzerland). For GC–MS analysis, the reaction mixture (3 μg NaAER1–0.5 mM benzalacetone) was incubated for 20 min at room temperature, and the product was extracted with 1 ml of ethyl acetate. Standard compound injections verified that the product of the NaAER1–benzalacetone reaction was benzylacetone.

Generation of promoter::eGFP lines and confocal imaging

Reporter lines were generated by transforming enhanced green fluorescent protein (eGFP) reporter plasmids to *N. attenuata* hypocotyl explants. Promoter sequences (2 kb upstream region from the *NaPAL4* and *NaPKS2* genes) were cloned into eGFP expressing binary plasmid derived from pH2GW7 (Karimi *et al.*, 2002). *Agrobacterium*-mediated transformation and tissue culture were performed as previously described, and three independent transformants for each line were investigated (Kang *et al.*, 2020). Transgenic flowers were fixed in 4% paraformaldehyde fixative containing 0.25% of glutaraldehyde, 0.1% of Triton X-100, and 0.1% of Tween 20 for overnight at 4°C. Samples were dehydrated and embedded in paraffin with a Leica EG1150H (Leica, Wetzlar, Germany). Cross-sections were cut at 10 μm using a microtome (Leica) and placed on slides, dried at 42°C. Sections were treated with xylene substitute to remove paraffin. Fluorescence signals were measured in flowers of regenerated reporter lines using an LSM780 confocal laser-scanning microscope (Carl

Zeiss, Oberkochen, Germany). Enhanced GFP was excited at 488 nm and emission signals were captured from 493 nm to 540 nm.

Results

Single-cell RNA sequencing defines distinct cell types in the corolla

To generate a single-cell transcriptome atlas of genes involved in BA biosynthesis, we isolated protoplasts from *N. attenuata* corolla limbs and throat cups at three time points (ZT 8, ZT 12, and ZT 16, one biological replicate) when BA emission increases (Fig. 1a). The protocol of protoplast isolation was optimized to retain cell integrity and the temporal transcriptome; the whole process, from flower excision to generating single-cell gel bead-in-emulsion, took *c.* 2 h. The 10x Genomics Chromium and the Illumina sequencing platforms were used to generate scRNA-Seq libraries. To evaluate the processes involved in scRNA-Seq, we generated a pseudo-bulk dataset for each time point by pooling scRNA-Seq UMIs and performed conventional bulk RNA-Seq with corolla limbs and throat cups collected at the same time points (ZT 8, ZT 12, and ZT 16, two biological replicates); these pseudo-bulk datasets were compared with the bulk RNA-Seq datasets. The global transcriptome profiles of two datasets were highly correlated (Pearson's correlation, $r > 0.8$, Supporting Information Fig. S1). We found several hypothetical proteins, ethylene-responsive factors, and zinc finger proteins that were highly induced in scRNA-Seq libraries compared to in bulk RNA-Seq results (Table S1, $\log_2$ FC > 5). Because the protoplast isolation process is known to induce several ethylene-responsive factors and zinc-finger proteins (Birnbaum *et al.*, 2003), we excluded genes that were consistently induced in three scRNA-Seq libraries from further analysis (Table S1). In single cell population, we detected 82–87% of genes that were detected in bulk RNA-Seq analysis (Fig. S2). A total of 16 465 genes detected in all time points was used for further analysis.

We next categorized single cells into clusters based on their shared transcriptomic profiles using the Seurat package (Satija *et al.*, 2015; Butler *et al.*, 2018). Cells from three time points were projected and visualized on a UMAP plot, which showed 10 distinct clusters in two-dimensional space (Figs 1b,c, S3). Because there were no well-known marker genes for flower cells, we assigned cell identities based on the putative biochemical functions of cluster-specific genes. The *N. attenuata* transcriptome was annotated based on the homology of protein-coding sequences to previously investigated genes in several model plants (Brockmöller *et al.*, 2017). For instance, in cluster 7, several pectin esterase genes, extension families, and homologs of pollen allergens were specifically detected; these cells were defined as pollen that had attached to the corolla's surface (Figs S4, S5). In cluster 8, we detected several orthologs of *AtSWEET11/12* and *AtSULTR2;1* genes, which are known to be specifically expressed in phloem and xylem (Figs S4, S7 see later) (Chen *et al.*, 2012; Maruyama-Nakashita *et al.*, 2015; Kim *et al.*, 2021).

We assigned the remaining major clusters to three groups of cells: epidermis, chlorenchyma, and parenchyma. Epidermal cells are known to express wax/cutin biosynthetic genes for synthesizing cuticular wax and cutin (Suh *et al.*, 2005). Several genes involved in cuticular wax biosynthesis were specifically enriched in clusters 0, 3, 4, 5, and 9: *ketoacyl-CoA synthase*, *ECERIFERUM4*, *wax ester synthase/diacylglycerol acyltransferase 1*, and several *lipid-transfer proteins*, which may participate in wax synthesis or transport, were highly expressed (Figs 1d, S6). We also found that clusters 0, 3, 4, 5, and 9 contained higher levels of cutin biosynthetic genes (*glycerol-3-phosphate acyltransferase 6* and *cutin synthase-like*) compared to other clusters; their protein sequences are similar to the well-studied orthologs of *Arabidopsis thaliana* (Fig. S7). These results suggest that clusters 0, 3, 4, 5, and 9 are epidermal cells. Cluster 6 was putatively defined as a chlorenchyma cell, because it contained highly expressed complex subunits of photosystems I and II (Figs 1e, S8). As shown in Fig. 1(a), the throat cup of the corolla retained chloroplasts. Photosynthetic genes are well-known to have a clear diurnal rhythm, with high levels during the day and low levels during the night (Kim *et al.*, 2011). Our scRNA-Seq data showed that the transcript levels of several photosynthetic genes gradually decreased from ZT 8 (in the middle of the day) to ZT 16 (reflecting the transition time from light to dark) (Fig. 1e). Clusters 1 and 2 had low levels of cuticle biosynthetic genes and relatively high levels of photosynthetic genes. These results suggest that in the corolla, clusters 1 and 2 are parenchyma cells.

Correlation analysis at single-cell resolution prioritizes candidate genes for benzylacetone biosynthesis

In the corolla, the initial step of BA biosynthesis is the nonoxidative deamination of Phe by the action of NaPAL4 (Fig. 2a) (Guo *et al.*, 2020). The product of NaPAL4 enzyme, *t*-cinnamic acid, is likely converted to cinnamoyl-CoA by a homologous protein of 4-coumarate:CoA ligase (4CL) or cinnamate:CoA ligase (CNL) (Klempien *et al.*, 2012) without further hydroxylation, because BA has no hydroxyl group on the aromatic ring. Next, we hypothesized that the cinnamoyl-CoA is likely condensed with one molecule of malonyl-CoA, which yields benzalacetone (4-phenyl-3-buten-2-one), a C_6–C_4 moiety of phenylbutanoid. Abe *et al.* (2001) found that a novel polyketide synthase named benzalacetone synthase produces 4-hydroxybenzalacetone (4-(4-hydroxyphenyl)-3-buten-2-one) from 4-coumaroyl-CoA and one molecule of malonyl-CoA in *R. palmatum* (Abe *et al.*, 2001; Morita *et al.*, 2010; Shimokawa *et al.*, 2012). *Nicotiana attenuata* contains four polyketide synthase enzymes (NaPKS1/2/3/4, renamed from NaCHAL1/2/3/4, respectively) homologous to chalcone synthase or benzalacetone synthase (Fig. S9) (Abe *et al.*, 2001); silencing *NaPKS*s in *N. attenuata* flowers dramatically reduces the level of BA emission (Kessler *et al.*, 2008; Guo *et al.*, 2020). In the target region of the previous RNA-interference (RNAi) construct, the *NaPKS3* (A4A49_39367) sequence differed from the *NaPKS1* (A4A49_08280), *NaPKS2* (A4A49_34074), and *NaPKS4* (A4A49_65921) sequences by only 34, 10, and 39 nucleotides, respectively (Kessler *et al.*, 2008)

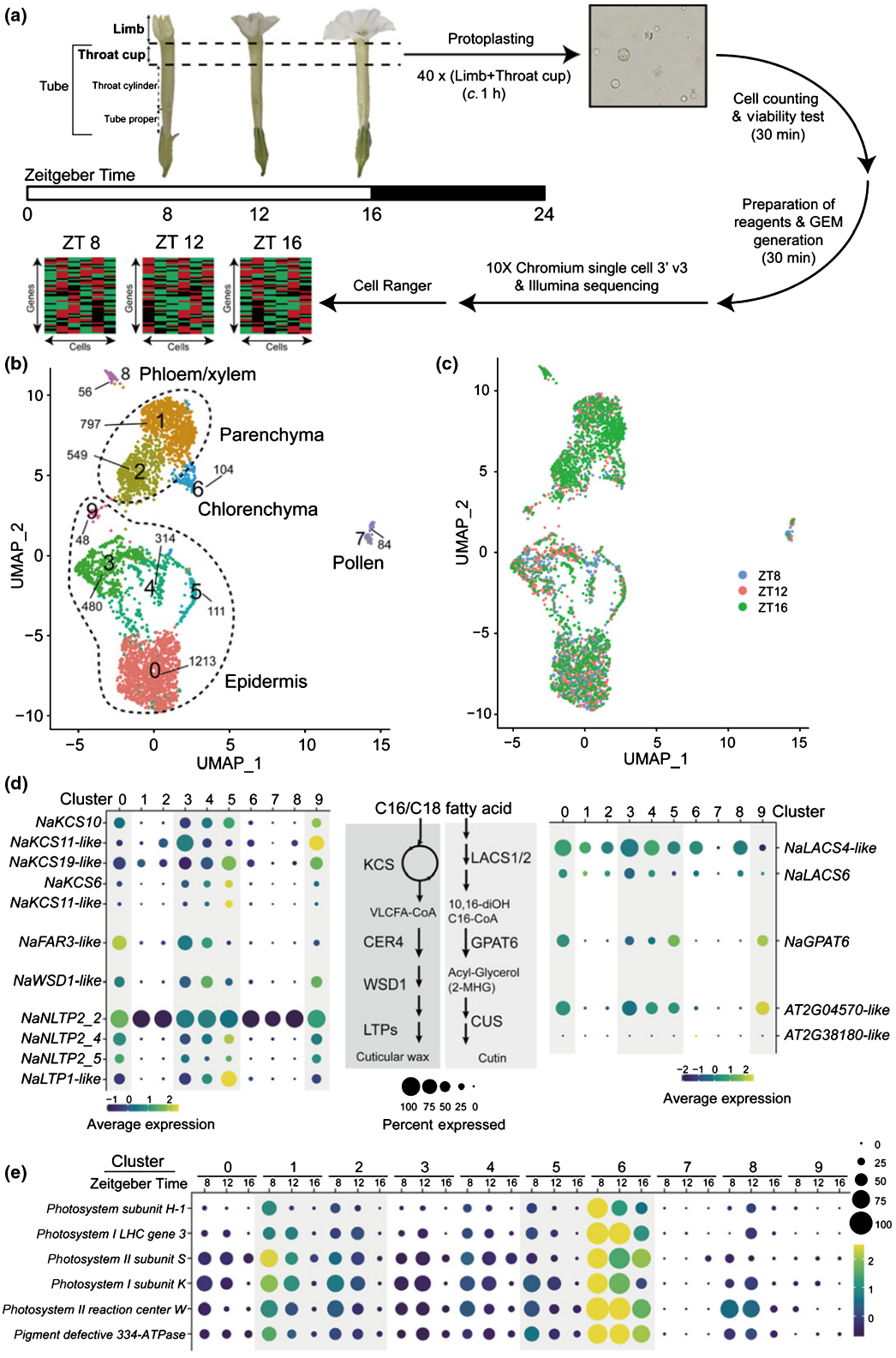

(Fig. S10). Therefore, we were not sure whether one or some NaPKSs help convert cinnamoyl-CoA to benzalacetone. Finally, benzalacetone appears to be reduced by an unknown reductase, which leads to the production of BA.

To identify BA biosynthetic genes, we hypothesized that all BA biosynthetic genes would be co-regulated over time at the single-cell level. Because NaPAL4 is known to be the first enzyme for BA biosynthesis, we calculated the Spearman's rank

Fig. 1 Single-cell RNA sequencing (scRNA-Seq) characterizes distinct *Nicotiana attenuata* corolla cell types. (a) Corolla limbs and throat cups were sampled from 40 *N. attenuata* flowers at each Zeitgeber Time (ZT), and scRNA-Seq libraries were generated. The total experimental procedures were finished within 2 h to reduce the effect of protoplasting. (b) A uniform manifold approximation and projection (UMAP) plot of the 3756 cells classified into five major cell types, composed of a total of 10 distinct clusters. The number of cells of each cluster is given next to clusters. (c) UMAP plot showing dimensional reduction of the distribution of 3756 corolla cells from three scRNA-Seq libraries. (d) Most biosynthetic genes of cuticular wax and cutin are highly enriched in clusters 0, 3, 4, 5, and 9. These genes are known to be expressed in the epidermis. CER4/FAR3, ECERIFERUM4/fatty acid reductase 3; CUS, cutin synthase-like; GPAT6, glycerol-3-phosphate acyltransferase 6; KCS, 3-ketoacyl-CoA synthase; LACS1/2, long-chain acyl-CoA synthase 1/2; LTP, lipid-transfer proteins; NLTP, nonspecific lipid-transfer proteins; VLCFA, very-long-chain fatty acids; WSD1, wax ester synthase/diacylglycerol acyltransferase 1. (e) Genes associated with photosynthesis are highly expressed in cluster 6 at all time points and in clusters 1, 2, and 6 at ZT 8. Photosynthetic genes have been reported to be expressed specifically in the inner layer cells, like mesophyll or parenchymal cells (Langdale & Nelson, 1991; Stockhaus *et al*., 1997).

correlation coefficient of *NaPAL4* expression with the whole gene expression detected in our scRNA-Seq data. For comparison, we also calculated the same gene-to-gene correlation in 20 previously published bulk RNA-Seq datasets from tissues including those of seed, leaf, root, stem, anther, style, stigma, ovary, nectary, pedicel, and corolla (Li *et al*., 2016; Brockmöller *et al*., 2017). We compared functional relationships among the top 40 ranked genes with *NaPAL4* in both datasets (Fig. 2b): genes involved in phenylpropanoid metabolism were detected more in scRNA-Seq (13 among 40 genes) than in bulk RNA-Seq (six among 40 genes).

Next, we prioritized candidate genes: CoA ligases, PKSs, and reductases in scRNA-Seq data based on the correlation with *NaPAL4*. The top 40 ranked genes in scRNA-Seq and bulk RNA-Seq data contained one common 4CL/CNL-like gene (Na4CL1, A4A49_40482), suggesting that Na4CL1 was the strongest candidate enzyme for producing BA. Among four *NaPKSs*, *NaPKS2* was the gene that ranked highest in scRNA-Seq datasets, followed by *NaPKS3* (Fig. 2c). However, in bulk RNA-Seq datasets, *NaPKS3* was correlated more with *NaPAL4* than was *NaPKS2* (Fig. 2c). Five homologs of 2-alkenal reductase (AER) and four homologues of isoflavone reductase (IFR), another family of reductases, were found in the scRNA-Seq and bulk RNA-Seq datasets. Interestingly, one putative AER (NaAER1, A4A49_31470) was highly ranked in scRNA-Seq (Fig. 2b,c). In the bulk RNA-Seq, all *IFR* genes and three of five *AER* homologs were more highly correlated with *NaPAL4* expression than was *NaAER1* (Fig. 2c). The distribution of the correlation coefficient in scRNA-Seq differed from its distribution in bulk RNA-Seq. A large number of genes in scRNA-Seq appeared to have a low correlation with *NaPAL4*: 99.46% of genes had a correlation coefficient between −0.25 and 0.25. The histogram from bulk RNA-Seq showed a broad and skewed distribution of correlation coefficients.

Na4CL1, NaPKS2, and NaAER1 are involved in benzylacetone biosynthesis

To test the model for BA biosynthesis that emerged from the co-expression analysis in scRNA-Seq datasets (Fig. 2a), we first silenced the expression of *Na4CL1* by VIGS and measured the level of floral volatiles in the headspace and in endogenous cells. Silencing *Na4CL1* reduced levels of BA both in the flower headspace (Fig. 3a) and in endogenous cells (Fig. 3b). It is noteworthy that other *Na4CL1* homologs (A4A49_41306 and A4A49_10638) and *NaCNL* homologs (A4A49_13610 and A4A49_12688), which are expressed in *N. attenuata* flowers, were not silenced in *Na4CL1*-silenced corolla (Figs S11, S12). To evaluate the catalytic ability of Na4CL1, purified Na4CL1 proteins were tested with *t*-cinnamic acid and several C_6–C_3 compounds (4-coumaric acid, caffeic acid, and ferulic acid) under the same conditions (Fig. 3c). Best-fit kinetic values were calculated by fitting with the Michaelis–Menten curve. Na4CL1 showed the ability to catalyze the formation of CoA-thioesters of *t*-cinnamic acid and similar C_6–C_3 compounds. Determined apparent Michaelis constant (K_M) values showed that Na4CL1 has a higher affinity to *t*-cinnamic acid and 4-coumaric acid than to caffeic acid and ferulic acid. Considering the catalytic rate constant (k_{cat}) values of *t*-cinnamic acid and derivatives, it seems that Na4CL1 can activate carboxylate groups in several C_6–C_3 compounds in *N. attenuata,* mediating reactions on carbon chains of phenylpropanoids. We next tried to clarify which NaPKSs were involved in BA biosynthesis. Although we designed the VIGS construct to be as specific as possible, the high sequence similarity observed among *NaPKSs* likely led to *NaPKS1*/*2*/*3*/*4* being silenced (Figs 4a, S10, S13). As previously reported, silencing *NaPKS*s reduced levels of BA in the headspace (Fig. 4a) and corolla limb (Fig. 4b). Although both *NaPKS2* and *NaPKS3* were strongly expressed in flower tissues (Fig. S14), scRNA-Seq datasets indicated that *NaPAL4* was more correlated with *NaPKS2* than with *NaPKS3* (Fig. 2c); *NaPAL4* and *NaPKS2* were mainly expressed in clusters 0, 3, and 4, but *NaPKS3* was expressed in the entire clusters (Fig. 6, see later). Interestingly, when we incubated the same amount of purified NaPKS2 or NaPKS3 proteins with Na4CL1 products (cinnamoyl-CoA) and malonyl-CoA (as carbon donor), we detected benzalacetone in the NaPKS2-containing mixture but not in the NaPKS3-containing mixture (Fig. 4c). The result suggests that NaPKS2 may play a major role for BA biosynthesis, as predicted by scRNA-Seq correlation analysis (Fig. 2c).

To identify the last step enzyme of BA biosynthesis, we silenced the candidate reductase *NaAER1* by VIGS and measured the level of floral volatiles in the headspace and in endogenous cells. Silencing *NaAER1* impaired BA biosynthesis in corollas without silencing other homologs; the levels of BA emission and endogenous BA were reduced in *NaAER1*-silenced flowers (Figs 5a,b, S15). We detected a novel compound emitted from *NaAER1*-silenced flowers, which was absent in headspace of control flowers (Fig. 5c). Metabolite fragmentation patterns and standard compound injections verified that this compound is

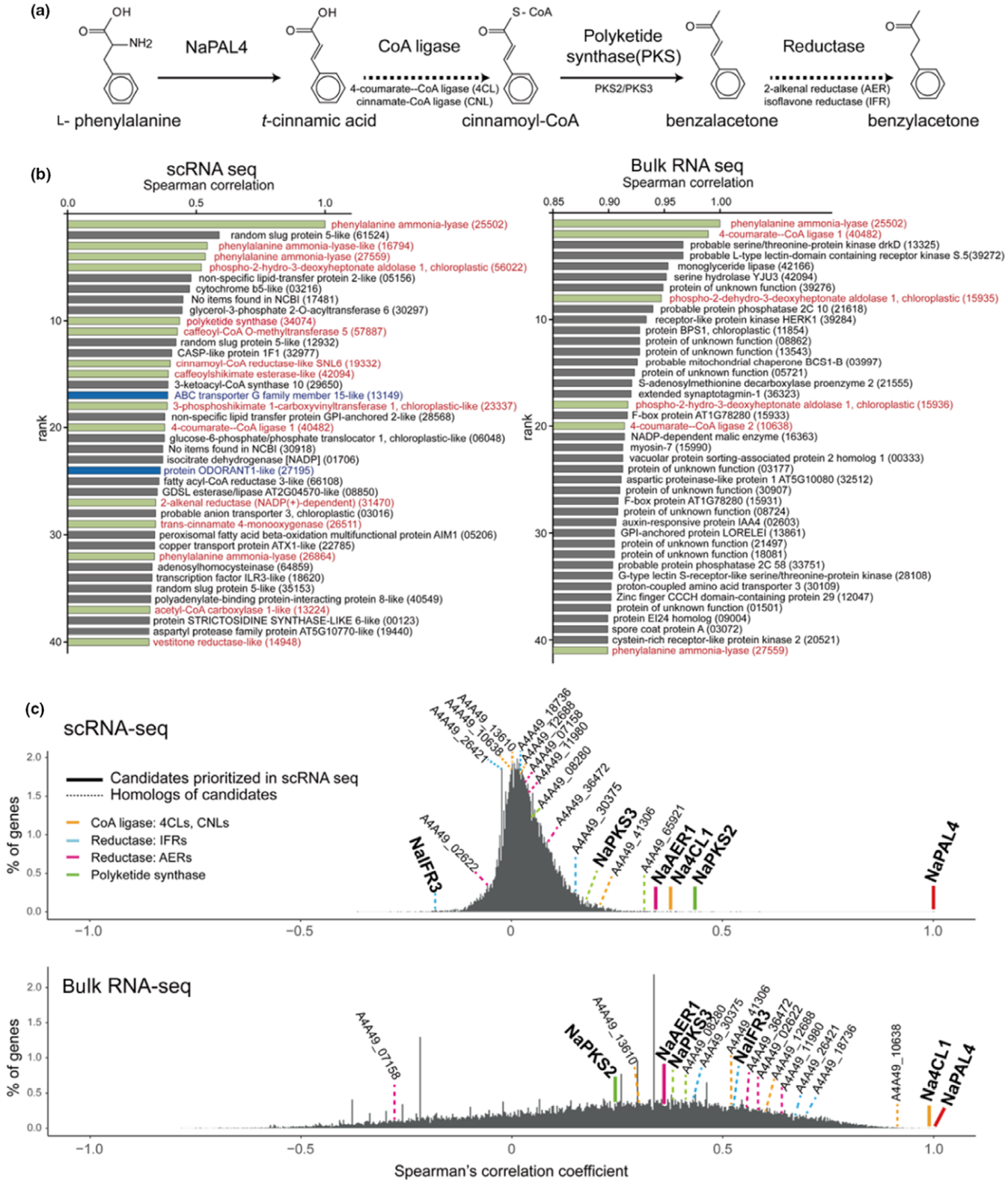

benzalacetone, the nonreduced form of BA. The kinetics analysis of NaAER1 proteins showed that benzalacetone had a lower K_M value than did other derivatives with hydroxyl or methoxy groups (Fig. 5d). Extinction coefficients used in NaAER1 kinetics were calculated experimentally: 6.314 l mmol^{-1} cm^{-1} for NADPH (340 nm), 0.6843 l mmol^{-1} cm^{-1} for benzalacetone (340 nm), 2.638 l mmol^{-1} cm^{-1} for NADPH (370 nm), 3.903 l mmol^{-1} cm^{-1} for 4-hydroxy-benzalacetone (370 nm), and 7.565 l

Fig. 2 Identification of benzylacetone (BA) biosynthetic genes via correlation analysis at single-cell resolution. (a) BA biosynthetic pathway proposed based on the biochemical function of NaPAL4 and NaPKS1/2/3/4 (solid lines), which has been characterized previously. Dashed lines indicate a putative reaction mediated by unknown enzymes: Coenzyme A (CoA) ligases and reductases; NaPAL4, *Nicotiana attenuata* phenylalanine ammonia-lyase 4; NaPKS, *N. attenuata* polyketide synthase. Genes tested in this study are annotated below the arrows. (b) Two correlation analyses display different top-ranked gene profiles. Genes are ranked by their correlation coefficients with NaPAL4. Single-cell RNA sequencing (scRNA-Seq) based analysis (left panel) generated more relevant profiles where several phenylpropanoid pathway associated genes were included; green bars: putative phenylpropanoid pathway genes, blue bars: homologs of transporter (ABC transporter) and transcription factor (ODORANT1) studied in petunia. (c) Percentage of genes (*y*-axis) that have a given Spearman's rank correlation coefficient (*x*-axis) with *NaPAL4* expression in scRNA-Seq and bulk RNA-Seq. Genes encoding CoA ligase, reductases, and polyketide synthases appear in different colors on the histograms. Thick lines highlight the CoA ligase, reductase, and polyketide synthase most correlated with *NaPAL4* in scRNA-Seq. NaAER1, *N. attenuata* 2-alkenal reductases 1; NaCNL, *N. attenuata* cinnamate:CoA ligase; NaIFR, *N. attenuata* isoflavone reductase; Na4CL1, *N. attenuata* 4-coumarate:CoA ligase.

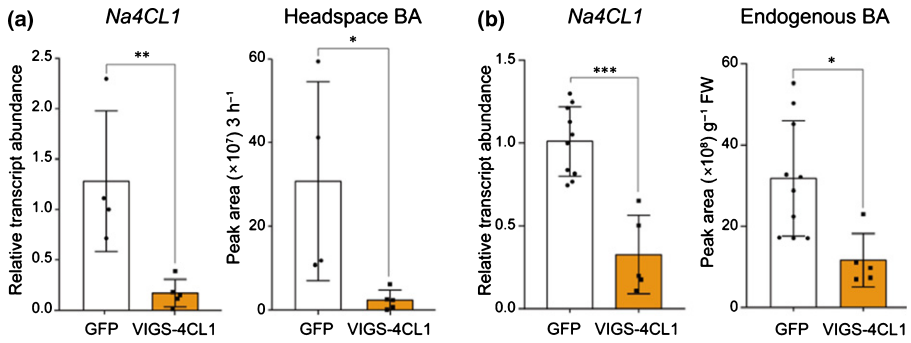

(c)

Substrate	*t*-cinnamic acid	*p*-coumaric acid	Caffeic acid	Ferulic acid
K_M (μM)	283.2 ± 125.5	104.2 ± 31.62	713.8 ± 395.6	529.7 ± 146.6
V_{max} (μM min^{-1})	38.4 ± 7.339	41.18 ± 4.019	88.85 ± 34.82	44.91 ± 6.566
k_{cat} (min^{-1})	339.8 ± 64.94	364.4 ± 35.56	786.1 ± 308.1	397.4 ± 58.09

Fig. 3 *Nicotiana attenuata* 4-coumarate:CoA ligase (Na4CL1) participates in benzylacetone (BA) biosynthesis in *N. attenuata* flowers. (a, b) Mean (± SD) levels of headspace BA and endogenous BA in corollas were measured in *Na4CL1*-silenced flowers (mean ± SD; *, $P < 0.05$; **, $P < 0.01$; ***, $P < 0.001$; two-tailed Student's *t*-test). Green fluorescent protein (GFP), plant infected TRV2:GFP (a truncated form), which was used as a negative control; VIGS-4CL1, a *Na4CL1*-silenced plant, which was generated by virus-induced gene silencing (VIGS). (c) Kinetic parameters (best-fit value ±SE) of Na4CL1 determined from *in vitro* enzyme assays of heterologously purified Na4CL1 protein. Best-fit catalytic values were calculated by fitting with the Michaelis–Menten curve, showing that Na4CL1 can catalyze the formation of Coenzyme A (CoA)-thioesters of *t*-cinnamic acid and similar C_6–C_3 compounds.

mmol^{-1} cm^{-1} for vanillylidenacetone (370 nm) (Fig. S16). Generalized Beer–Lambert laws for complex mixtures were adopted for calculating decreasing amounts of substrates (Wypych, 2015). In addition, GC–MS confirmed that purified NaAER1 proteins with NADPH, a biological reducing agent, can convert benzalacetone to BA (Fig. S17). The accumulation of benzalacetone in *NaAER1*-silenced corollas and the *in vitro* assay showed that NaAER1 is the final enzyme involved in BA biosynthesis.

Recently, Guo *et al.* (2020) reported that *NaIFR3* correlated strongly with *NaPAL4* in the same bulk RNA-Seq dataset used in this study. Although we also observed the positive correlation between *NaIFR3* and *NaPAL4* in bulk RNA-Seq data, there was no positive correlation between these two genes in the scRNA-Seq dataset (Fig. 2c). Furthermore, we found that levels of BA emission in *NaIFR3*-silenced corollas did not differ significantly from levels in control corollas (Fig. S18a), even though the silencing efficacy of *NaIFR3* in our study was approximately three-fold higher than in the previous study (Guo *et al.*, 2020). Because there was a large variation in BA emission from *NaIFR3*-silenced corollas, we measured the endogenous levels of BA in control and *NaIFR3*-silenced corollas. No difference in endogenous BA levels with a low variation was found between control and *NaIFR3*-silenced corollas (Fig. S18b).

Benzylacetone is synthesized in the epidermal layer

Among the 3756 cells, 1648 contained at least one molecule of *NaPAL4* messenger RNA (mRNA) (Fig. S19). Given that 80% of *NaPAL4*-expressing cells belonged to epidermal cells (clusters 0, 3, and 4), we hypothesize that BA is synthesized in the epidermal layer of the corolla. We calculated the number of cells harboring individual gene or combination of *NaPAL4*, *Na4CL1*, *NaPKS2*, and *NaAER1* genes. Of 3756 cells, 1097 contained all four genes; 94% of these cells were found in clusters 0, 3, and 4 (epidermal cells) (Fig. 6a). Most *NaPAL4*-expressing cells (67%) contained all three genes: *Na4CL1*, *NaPKS2*, and *NaAER1*. To visualize the spatial distribution of cells in which two target genes were co-expressed, we merged two featureplots of *NaPAL4* and one of *Na4CL1*, *NaPKS2*, and *NaAER1* expression (Fig. 6b). The results showed that a high level of co-expression (yellowish cells) was mainly found in cluster 0, implicating the scent-biosynthesis step that occurs in the epidermis. To validate the

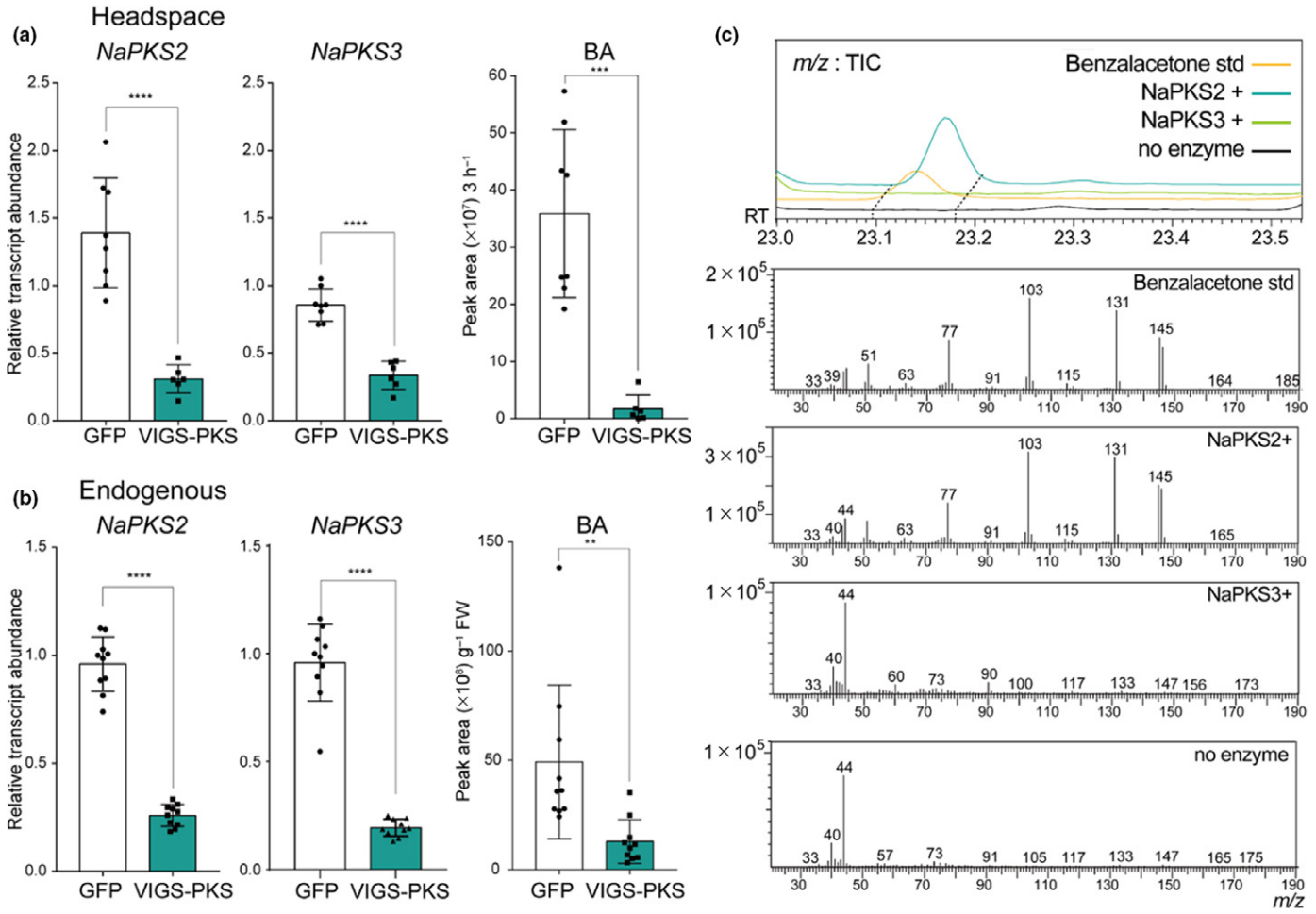

Fig. 4 *Nicotiana attenuata* polyketide synthase 2 (NaPKS2) is the enzyme that participates in benzylacetone (BA) biosynthesis in *N. attenuata* flowers. (a) *NaPKS2* and *NaPKS3* are co-silenced in *NaPKS2/3*-silenced corollas. Green fluorescent protein (GFP), plant infected TRV2-GFP (a truncated form), which was used as a negative control; VIGS-PKS, a *NaPKSs* co-silenced plant, which was generated by virus-induced gene silencing (VIGS) (mean ± SD; **, $P < 0.01$; ***, $P < 0.001$; ****, $P < 0.0001$; two-tailed Student's *t*-test). Mean (±SD) levels of headspace BA show that *NaPKS2/3*-silenced flowers emit less BA. (b) *NaPKS2/3*-silenced flowers harbor less endogenous BA in corolla tissue. (mean ± SD; **, $P < 0.01$; ***, $P < 0.001$; ****, $P < 0.0001$; two-tailed Student's *t*-test). (c) *In vitro* enzyme assay reveals that NaPKS2, not NaPKS3, can synthesize benzalacetone, a putative intermediate of BA biosynthesis. A novel peak detected in NaPKS2-contained reaction mixtures represents benzalacetone, based on its fragmentation pattern and standard compound injections.

location of BA-biosynthetic cells, we generated *NaPAL4* promoter-GFP lines and *NaPKS2* promoter-GFP lines in *N. attenuata*. In both lines, GFP expression was strongly detected in the corolla epidermis, especially in the adaxial region (Fig. S20), which suggests that clusters 0, 3, and 4 are the epidermal cells. Phe biosynthetic genes were detected mainly in clusters 0, 3, and 4, but these genes were also expressed in other clusters (clusters 1 and 2) (Fig. 6c). Dotplots also showed that *NaPAL2/3/4* with *Na4CL1*, *NaPKS2*, and *NaAER1* were highly expressed in the epidermal cells (Fig. 6c).

Diurnal rhythms of benzylacetone (BA) biosynthetic genes and BA emissions

Because *N. attenuata* flowers emit BA rhythmically (Yon *et al.*, 2016), we asked whether all BA biosynthetic genes share this diurnal expression pattern. In our experiments, BA emission began to increase near ZT 12 and peaked at ZT 16 (Fig. 7a). Quantitative PCR analysis showed that the transcript levels of *NaPAL4*, *Na4CL1*, *NaPKS2*, and *NaAER1* peaked *c.* 4 h before BA emission levels peaked, suggesting that BA emission is regulated mainly at the transcriptional level. The scRNA-Seq data also showed similar expression patterns of BA biosynthetic genes. For instance, the violin plots illustrated a similar time-dependent expression of *NaPAL4* transcripts in clusters 0, 3, and 4 (Fig. 7b). The transcript levels of the other BA biosynthetic genes in each cluster also depended on time with slight differences: *Na4CL1* and *NaAER1* expression peaked at ZT 12 in all clusters, but *NaPKS2* expression increased from ZT 8 to ZT 16 in the epidermal clusters only (Fig. 7b).

In petunia flowers, rhythmic scent emission is regulated by several transcriptional activators: *Petunia×hybrida ODORANT1* (*PhODO1*) and *EMISSION OF BENZENOID I/II* (*PhEOBI/II*) (Dexter *et al.*, 2007; Klempien *et al.*, 2012; Fenske *et al.*, 2015;

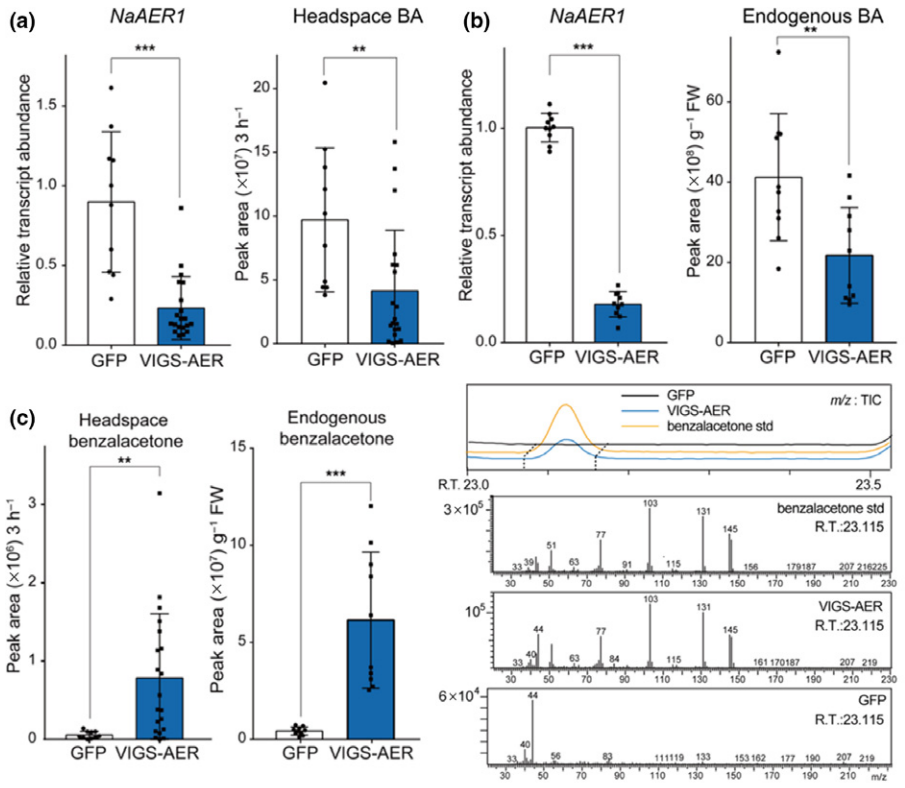

(d)

Substrate	Benzalacetone	4-hydroxy-benzalacetone	Vanillylidenacetone
K_M (μM)	82.36 ± 36.46	681.2 ± 127.9	3.07×10^{17}
V_{max} (μM min^{-1})	5.57 ± 0.9313	25.73 ± 2.809	5.833×10^{15}
k_{cat} (min^{-1})	9.403 ± 1.572	43.43 ± 4.742	Ambiguous

Fig. 5 *Nicotiana attenuata* 2-alkenal reductase 1 (NaAER1) catalyzes the final step in benzylacetone (BA) biosynthesis. (a, b) Mean (± SD) levels of headspace BA and endogenous BA measured in *NaAER1*-silenced flowers (mean ± SD; **, $P < 0.01$; ***, $P < 0.001$; two-tailed Student's *t*-test). BA levels were reduced in *NaAER1*-silenced flowers. Green fluorescent protein (GFP), plant infected TRV2-GFP (a truncated form), which was used as a negative control; VIGS-AER, a *NaAER1*-silenced plant, which was generated by virus-induced gene silencing (VIGS). (c) Benzalacetone, a metabolic intermediate of BA, was emitted from *NaAER1*-silenced flowers and not from control flowers (mean ± SD; **, $P < 0.01$; ***, $P < 0.001$; two-tailed Student's *t*-test). Right panel shows a novel gas chromatography–mass spectrometry (GC–MS) peak in headspace of a *NaAER1*-silenced flower, which has the same retention time and mass fragmentation pattern as the benzalacetone standard. (d) Kinetic parameters (best-fit value ± SE) of NaAER1 determined from *in vitro* enzyme assays of heterologously purified NaAER1 protein. Best-fit catalytic values were calculated by fitting with the Michaelis–Menten curve.

Amrad *et al.*, 2016). *PhODO1* peaks in the evening, right before scent emission peaks (Verdonk *et al.*, 2005; Spitzer-Rimon *et al.*, 2013). *PhEOBII* peaks in the morning (Spitzer-Rimon *et al.*, 2010), and directly activates *PhODO1* and *PhEOBI*. (Van Moerkercke *et al.*, 2011). In the *N. attenuata* genome database, we identified several homologs of three petunia MYB transcription factors (Brockmöller *et al.*, 2017). Among these homologs, we found that one homolog of *PhODO1* and two homologs of *PhEOBI/II* were expressed in *N. attenuata* flowers. The amino acid sequence alignment between *N. attenuata* and petunia is shown in Fig. S21. Quantitative PCR analysis showed that *NaODO1-like* and *NaEOBI-like* peaked concurrently with BA biosynthetic genes (ZT 12), and *NaEOBII-like* peaked during the daytime (Fig. 7a); these transcript dynamics were also observed in the violin plots (Fig. 7b). Single-cell RNA-Seq data showed that *NaODO1-like* expression rather than *NaEOBI/II* had a high correlation with *NaPAL4* (Fig. 2b) and was confined to clusters 0, 1, 2, 3, and 4, which suggests that *NaODO1-like* regulates BA biosynthetic genes.

Next, we measured transcript levels of BA biosynthetic genes in the corolla limb and tube (Fig. 7c). Although transcript levels of *NaPAL4* in the corolla limb did not differ with the level in the corolla tube, *Na4CL1* expression was lower in the corolla tube than in the corolla limb. The *NaPKS2* and *NaAER1* transcripts were barely detected in the corolla tube, which is consistent with the known location of BA biosynthesis (Euler & Baldwin, 1996; Kessler & Baldwin, 2007).

Discussion

BA is synthesized mainly in epidermal cells, as revealed from how cell populations clustered and from the spatial distribution of BA

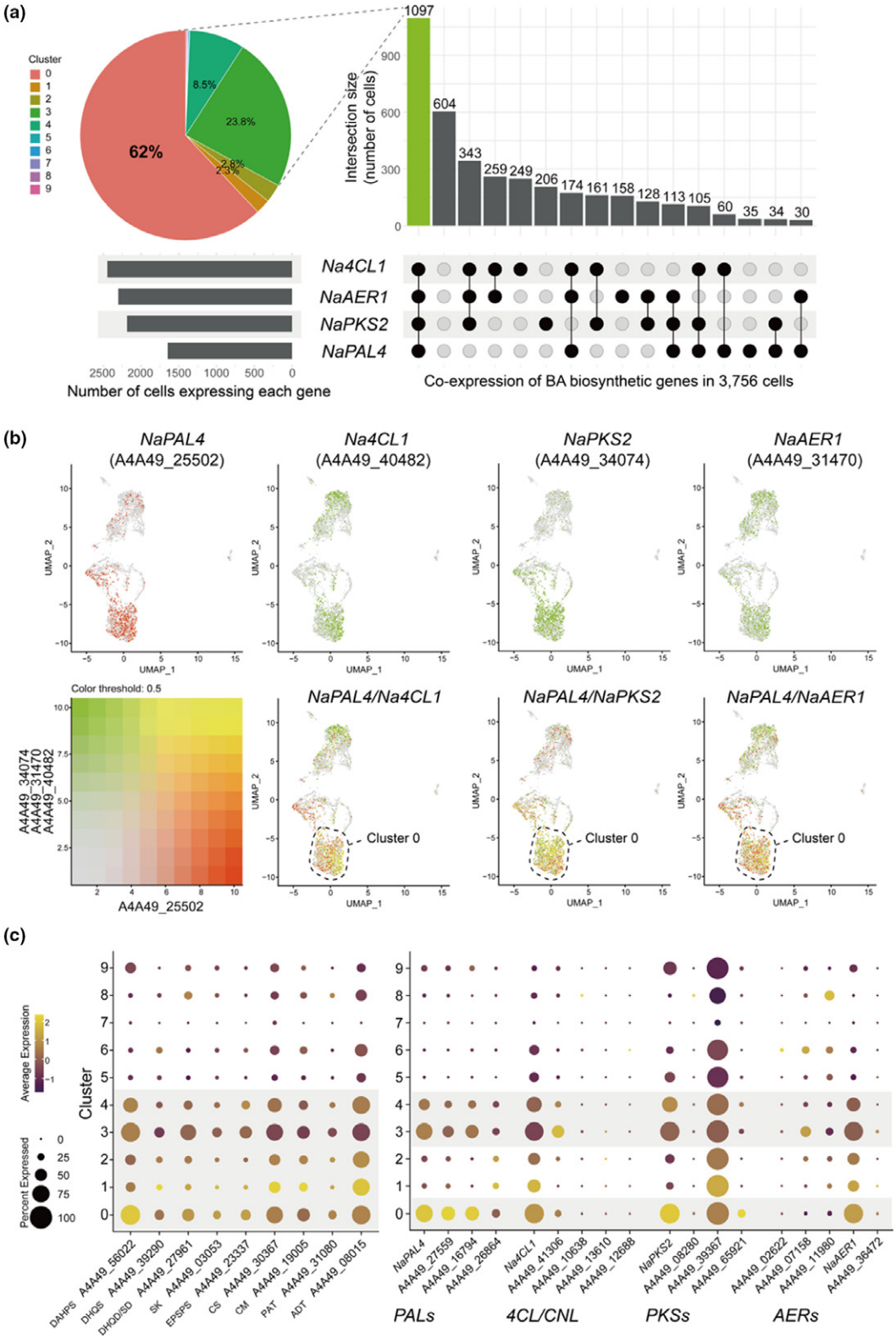

biosynthetic genes. NaPAL4, the first enzyme required for BA biosynthesis, was found in the epidermis (Fig. S20). Most cells (67%) expressing *NaPAL4*, the gene required for the initial step in BA biosynthesis, harbored all other BA biosynthetic genes, indicating that the single-cell transcriptome map of *NaPAL4* largely concurred with the map of BA-producing cells in the corolla. Only 45% of *Na4CL1*-, 50% of *NaPKS2*-, and 48% of *NaAER1*-expressing cells contained the entire set of BA

Fig. 6 Characterization of benzylacetone (BA) biosynthetic cell clusters. (a) An UpSet plot shows numbers of cells harboring individual gene or combination of *NaPAL4*, *Na4CL1*, *NaPKS2*, and *NaAER1* genes. A pie chart represents the distribution of clusters of cells expressing all four genes. Clusters 0, 3, and 4 (epidermis) contain 94.3% of cells co-expressing all four genes. (b) Featureplots visualize co-expression between *NaPAL4* and *Na4CL1*, *NaPKS2*, and *NaAER1*, respectively. Cells that co-express genes mostly locate in cluster 0. (c) Dotplots of L-phenylalanine (Phe) biosynthetic genes (primary metabolism) and BA biosynthetic genes (secondary metabolism). Phe is mainly synthesized in clusters 0 to 4, and BA synthesis occurs in clusters 0, 3, and 4. NaPAL4, *Nicotiana attenuata* phenylalanine ammonia-lyase 4; Na4CL1, *N. attenuata* 4-coumarate:CoA ligase; NaPKS2, *N. attenuata* polyketide synthase 2; NaAER1, *N. attenuata* 2-alkenal reductase 1; DAHPS, phospho-2-dehydro-3-deoxyheptonate aldolase; DHQS, 3-dehydroquinate synthase; DHQD/SD, bifunctional 3-dehydroquinate dehydratase/shikimate dehydrogenase; SK, shikimate kinase; EPSPS, 3-phosphoshikimate 1-carboxyvinyltransferase 1; CS, chorismate synthase; CM, chorismate mutase; PAT, bifunctional aspartate aminotransferase and glutamate/aspartate-prephenate aminotransferase; ADT, arogenate dehydratase/prephenate dehydratase.

biosynthetic genes. High levels of *NaPAL4* and *Na4CL1* transcripts were found in the corolla limb and in the corolla tube (Fig. 7c), although no BA is produced in the tube. In contrast, *NaPKS2* and *NaAER1* transcripts were detected in the corolla limb and not in the tube, suggesting that the expression of *NaPKS2* and *NaAER1* determines BA production at the suborgan level. Phe biosynthetic genes were mainly found in the epidermal clusters (Fig. 6c), which suggests that primary metabolism in corollas is specialized to support the high demands of secondary metabolite production.

Transcriptional heterogeneity, both in different plant tissues and amongst accessions with distinctive floral volatile productions, has been used to identify key enzymes for volatile biosynthesis. Bulk RNA-Seq analysis is a powerful method with which to examine gene-to-gene correlation in several samples (Boachon *et al.*, 2015, 2019; Xu *et al.*, 2018). In addition, bulk RNA-Seq analysis is useful for predicting a target gene among several homologous genes in plant tissues (Wong *et al.*, 2020): *Petunia CNL* gene was identified by sequence comparison and bulk RNA-Seq analysis (Klempien *et al.*, 2012). We analyzed publicly available bulk RNA-Seq datasets containing 14 different tissues from *N. attenuata,* because BA is synthesized in the corolla but not in other tissues. The metabolic heterogeneity among these tissues was used to identify a CoA ligase, Na4CL1, in BA biosynthesis (Fig. 2). However, the bulk RNA-Seq datasets used in this study were insufficient for exploring the entire BA biosynthetic pathway, perhaps because *NaPAL4* expressed in other plant tissues may be involved in other phenylpropanoid pathway.

A previous study (Guo *et al.*, 2020) has suggested a BA biosynthetic pathway that differs from our biosynthetic pathway. Guo *et al.* (2020) suggested that *t*-cinnamic acid is condensed with one malonyl-CoA by an unknown CoA ligase and malonyl transferase; the malonylated compound is then reduced by NaIFR3, and the acyl side chain of the reduced compound is removed by NaPKS3. Here, we propose that NaPKS2 condenses cinnamoyl-CoA with one malonyl-CoA to form benzalacetone; no additional malonyl transferase is necessary for BA biosynthesis. Although the protein sequence of NaPKS2 shared a high similarity with NaPKS3, scRNA-Seq analysis predicts that NaPKS2 is the key enzyme for BA biosynthesis. Purified NaPKS2 proteins produced benzalacetone from the mixture of cinnamoyl-CoA and malonyl-CoA (Fig. 4c). Although purified NaPKS3 proteins produced no benzalacetone *in vitro*, more genetic evidence is needed to examine the biochemical function of NaPKS3 *in vivo*. We also propose that NaAER1 is the major reductase for BA biosynthesis; the levels of BA in the headspace and in endogenous corolla cells were lower in *NaAER1*-silenced corollas than in control corollas. The nonreduced form of BA was found in the headspace and in endogenous cells of *NaAER1*-silenced corollas. Although Guo *et al.* (2020) showed that *NaIFR3*-silenced flowers emitted less BA than did control flowers, we found that silencing *NaIFR3* did not alter the headspace and endogenous levels of BA in the corollas. *NaIFR3* expression was shown to be highly correlated with *NaPAL4* expression in the bulk RNA-Seq dataset, but not in the scRNA-Seq dataset (Figs 2c, S22). *NaAER1* was more correlated with *NaPAL4* than was *NaIFR3* in the scRNA-Seq dataset (Fig. 2). This discrepancy may have originated from the large variation in the headspace levels of BA emitted from *NaIFR3*-silenced corollas (Fig. S18) and the unintended sample selection bias in the previous study. Members of an IFR family are known to bind a flavonoid, which has a C_6–C_3–C_6 carbon skeleton (Wang *et al.*, 2006; Cheng *et al.*, 2015). Silencing *NaIFR3*, which may alter the level of flavonoids, affects BA emission but not BA biosynthesis.

We analyzed the transcriptomic profiles of corolla at the single cell level, which reveals the existence of distinctive cell identities in *N. attenuata* corolla cells. This cell-to-cell heterogeneity in the corolla helps us to identify unknown BA biosynthetic genes. To increase cell heterogeneity, we performed more time-point sampling rather than biological replicate sampling. Our major aim was to identify floral scent (BA) biosynthetic genes using gene-to-gene correlation. We thought that time-series sampling is useful to increase the power of correlation analysis, because *N. attenuata* flowers synthesize BA diurnally (Fig. 7). That is why we performed scRNA-Seq experiments at three different time points instead of using three biological replicates. Rather than retrieving the average transcript levels of genes in tissue, we can examine gene-to-gene correlation using the transcript levels of genes expressed in a single cell. However, the lack of replicates may weaken the correlation analysis because we were not able to differentiate between technical noise and biological variability.

Single-cell RNA-Seq generates high-dimensional data, which may provide more reliable correlation among genes (Shinozaki *et al.*, 2018). Bulk RNA-Seq data contain tens of thousands of variables (gene number), but the number of samples is much smaller than the number of genes. However, the scRNA-Seq data have thousands of variables (gene numbers) with large numbers of cells. It is noteworthy to mention that scRNA-Seq, which can only detect a thousand genes in a single cell, might contain

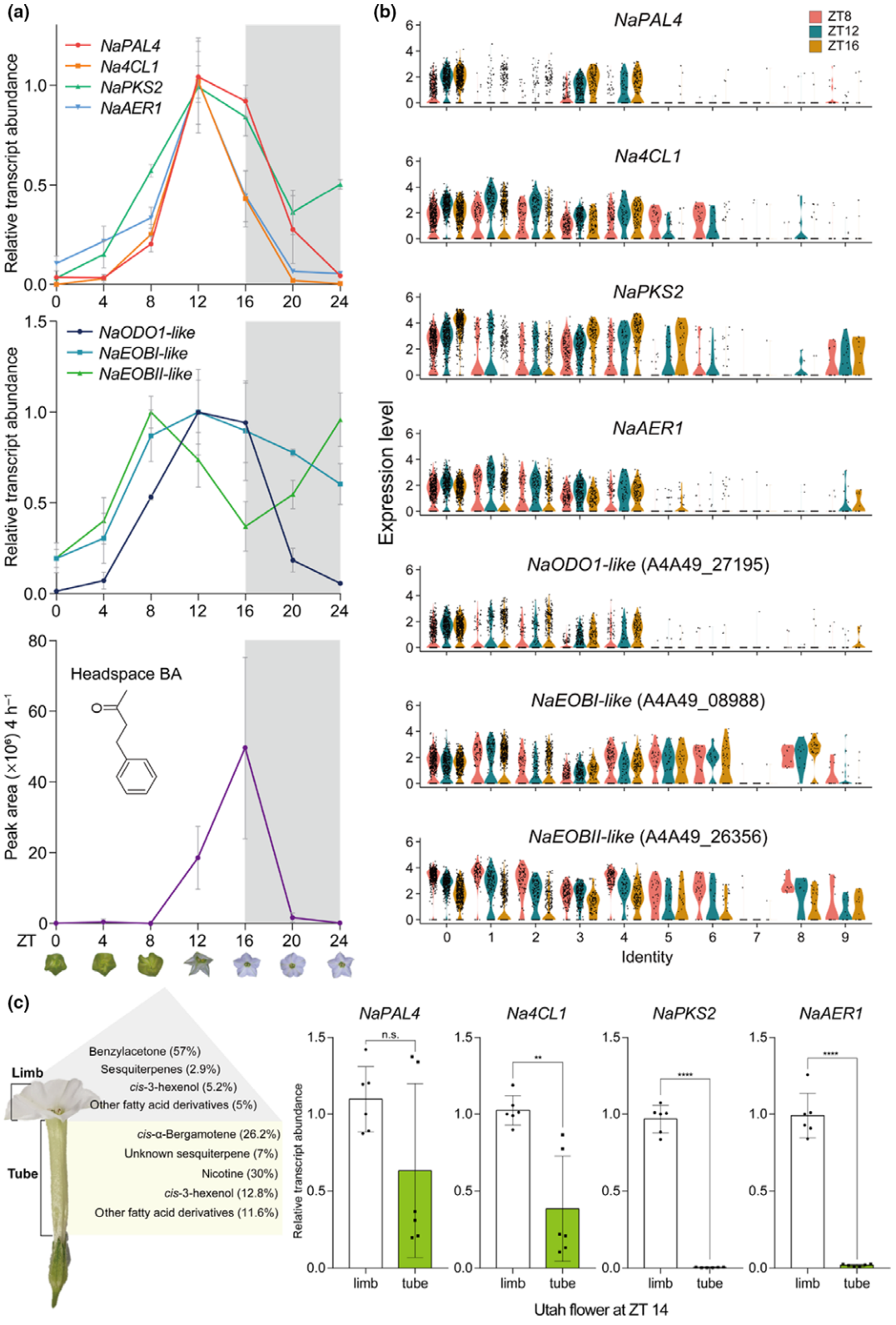

numerous false zeros in a matrix. Bulk RNA-Seq, in contrast, can capture over 10 000 genes in a sample; with proper sampling design, bulk RNA-Seq can improve the identification of biosynthetic genes. In addition, our protoplasting method may provoke cell-type-dependent dissociation, which can be solved by single-nucleus RNA-Seq (Wu *et al.*, 2019). Although gene co-expression analysis of scRNA-Seq data is limited by low sequencing depth per cell (dropout events) and a high level of technical noise, scRNA-Seq analysis can be used to investigate biosynthetic genes of a target metabolite.

Fig. 7 Diurnal rhythm of benzylacetone (BA) biosynthesis genes and its expression pattern in flower tissues. (a) Rhythmic emission of BA and expression of related genes. Relative transcript levels (mean ± SD) of *NaPAL4*, *Na4CL1*, *NaPKS2*, and *NaAER1* peak at Zeitgeber Time (ZT) 12, 4 h before the peak of BA emission. *NaODO1-like* and *NaEOBI-like* also peak at ZT 12 when the BA synthesis genes peak, and *NaEOBII-like* peaks 4 h earlier than other MYP transcription factors. *NaEOBI/II-like*, *Nicotiana attenuata EMISSION OF BENZENOID I/II-like*; *NaODO1-like*, *N. attenuata ODORANT1-like*. (b) Violin plots show the expression levels of BA biosynthetic genes and MYB transcription factors across all clusters at three different time points. The levels of *Na4CL1* and *NaAER1* transcript peak at ZT 12 (widest sections of violin plots are higher than ZT 8 and ZT 16), as shown in (a). *NaPAL4* and *NaPKS2* transcript levels at ZT 16 are higher than those at ZT 8 and 12 in clusters 0, 3, and 4. Violin plots of MYB transcription factors also reflect transcriptional dynamics shown in (a). (c) Kessler & Baldwin (2007) reported the percentage of *N. attenuata* floral scents in the floral headspace. BA is synthesized mainly in the corolla limb, and *cis*-α-bergamotene is synthesized in the corolla tube. Quantitative transcript analysis of BA biosynthetic genes in dissected flower tissues of limb and tube reveals that the lack of BA emission in the corolla tube resulted from the limited expression of *NaPKS2* and *NaAER1* (mean ± SD; n.s., not significant, **, $P < 0.01$; ****, $P < 0.0001$; two-tailed Student's *t*-test). NaPAL4, *N. attenuata* phenylalanine ammonia-lyase 4; Na4CL1, *N. attenuata* 4-coumarate:CoA ligase; NaPKS2, *N. attenuata* polyketide synthase 2; NaAER1, *N. attenuata* 2-alkenal reductase 1.

Recent technological advances, such as live single-cell MS enable us to examine metabolic profiling in single cells (Fujii *et al.*, 2015). Apparent cell types like trichomes or guard cells have been extensively studied for their single-cell-type metabolism (Misra *et al.*, 2014). However, it is hard to measure levels of a metabolite of low abundance within a single cell. The detection of intermediates is also difficult due to their rapid turnover rates. For instance, we were not able to detect benzalacetone (BA intermediate) in *N. attenuata* headspace. In this study, without the measurement of BA intermediate, we were able to identify benzalacetone synthase (*NaPKS2*) and reductase (*NaAER1*) in the corolla. This result suggests that scRNA-Seq analysis coupled with single-cell metabolite analysis will enhance our understanding of metabolic heterogeneity and pathways in a single cell.

Acknowledgements

The authors appreciate Dr Inkyung Jung, Seongwan Park, and Mooyoung Kim for helping them to generate a scRNA-Seq library; Dr Gisuk Lee and Dr Yongsung Joo for help with metabolite analysis; San-Hae Lim with protein purification; Guo Han, Shuqing Xu, and Ian T. Baldwin for comments on BA biosynthetic pathway; Emily Wheeler for editorial assistance. This work is supported by grants from the Samsung Science & Technology Foundation (SSTF-BA1901-10, S-GK) and TJ Park Doctoral Science Fellowship (MK). The authors declare no competing interests.

Author contributions

S-GK conceived and supervised the project. MK generated scRNA-Seq libraries and performed bioinformatic analysis. YC generated cDNA libraries for bulk RNA- Seq. MK and HK analyzed plant volatiles. MK and HK performed VIGS experiments. MK conducted quantitative PCR analysis and *in vitro* enzyme assay. S-GK and MK wrote the manuscript.

ORCID

Yuri Choi https://orcid.org/0000-0002-7704-4269
Moonyoung Kang https://orcid.org/0000-0002-4630-4312
Hyeonjin Kim https://orcid.org/0000-0001-9054-3874
Sang-Gyu Kim https://orcid.org/0000-0003-2574-3233

Data availability

Single-cell RNA-Seq data discussed in this publication have been deposited in NCBI's Gene Expression Omnibus and are accessible through GEO series accession no. GSE193464. Other data generated during this study are included in this published article and Supporting Information files.

References

Abe I, Takahashi Y, Morita H, Noguchi H. 2001. Benzalacetone synthase. A novel polyketide synthase that plays a crucial role in the biosynthesis of phenylbutanones in *Rheum palmatum*. *European Journal of Biochemistry* **268**: 3354–3359.

Amrad A, Moser M, Mandel T, de Vries M, Schuurink RC, Freitas L, Kuhlemeier C. 2016. Gain and loss of floral scent production through changes in structural genes during pollinator-mediated speciation. *Current Biology* **26**: 3303–3312.

Baldwin IT, Preston C, Euler M, Gorham D. 1997. Patterns and consequences of benzyl acetone floral emissions from *Nicotiana attenuata* plants. *Journal of Chemical Ecology* **23**: 2327–2343.

Barkman TJ, Martins TR, Sutton E, Stout JT. 2007. Positive selection for single amino acid change promotes substrate discrimination of a plant volatile-producing enzyme. *Molecular Biology and Evolution* **24**: 1320–1329.

Baudino S, Hugueney P, Caissard J-C. 2020. Chapter 12: evolution of scent genes. In: Pichersky E, Dudareva N, eds. *Biology of plant volatiles*. Boca Raton, FL, USA: CRC Press.

Birnbaum K, Shasha DE, Wang JY, Jung JW, Lambert GM, Galbraith DW, Benfey PN. 2003. A gene expression map of the *Arabidopsis* root. *Science* **302**: 1956–1960.

Boachon B, Burdloff Y, Ruan JX, Rojo R, Junker RR, Vincent B, Nicolè F, Bringel F, Lesot A, Henry L *et al.* 2019. A promiscuous CYP706A3 reduces terpene volatile emission from *Arabidopsis* flowers, affecting florivores and the floral microbiome. *Plant Cell* **31**: 2947–2972.

Boachon B, Junker RR, Miesch L, Bassard JE, Höfer R, Caillieaudeaux R, Seidel DE, Lesot A, Heinrich C, Ginglinger JF *et al.* 2015. CYP76C1 (Cytochrome P450)-mediated linalool metabolism and the formation of volatile and soluble linalool oxides in *Arabidopsis* flowers: a strategy for defense against floral antagonists. *Plant Cell* **27**: 2972–2990.

Brockmöller T, Ling Z, Li D, Gaquerel E, Baldwin IT, Xu S. 2017. *Nicotiana attenuata* Data Hub (*Na*DH): an integrative platform for exploring genomic, transcriptomic and metabolomic data in wild tobacco. *BMC Genomics* **18**: 1–11.

Butler A, Hoffman P, Smibert P, Papalexi E, Satija R. 2018. Integrating single-cell transcriptomic data across different conditions, technologies, and species. *Nature Biotechnology* **36**: 411–420.

Chen H, Li G, Köllner TG, Jia Q, Gershenzon J, Chen F. 2014. Positive Darwinian selection is a driving force for the diversification of terpenoid biosynthesis in the genus *Oryza*. *BMC Plant Biology* **14**: 1–12.

Chen LQ, Qu XQ, Hou BH, Sosso D, Osorio S, Fernie AR, Frommer WB. 2012. Sucrose efflux mediated by SWEET proteins as a key step for phloem transport. *Science* **335**: 207–211.

Cheng Q, Li N, Dong L, Zhang D, Fan S, Jiang L, Wang X, Xu P, Zhang S. 2015. Overexpression of soybean isoflavone reductase (*GmIFR*) enhances resistance to phytophthora sojae in soybean. *Frontiers in Plant Science* **6**: 1–11.

Denyer T, Ma X, Klesen S, Scacchi E, Nieselt K, Timmermans MCP. 2019. Spatiotemporal developmental trajectories in the *Arabidopsis* root revealed using high-throughput single-cell RNA sequencing. *Developmental Cell* **48**: 840–852.e5.

Dexter R, Qualley A, Kish CM, Ma CJ, Koeduka T, Nagegowda DA, Dudareva N, Pichersky E, Clark D. 2007. Characterization of a petunia acetyltransferase involved in the biosynthesis of the floral volatile isoeugenol. *The Plant Journal* **49**: 265–275.

Dudareva N, Cseke L, Blanc VM, Pichersky E. 1996. Evolution of floral scent in *Clarkia*: novel patterns of S-linalool synthase gene expression in the *C. breweri* flower. *Plant Cell* **8**: 1137–1148.

Dudareva N, Pichersky E. 2000. Biochemical and molecular genetic aspects of floral scents. *Plant Physiology* **122**: 627–634.

Euler M, Baldwin IT. 1996. The chemistry of defense and apparency in the corollas of *Nicotiana attenuata*. *Oecologia* **107**: 102–112.

Fenske MP, Hewett Hazelton KD, Hempton AK, Shim JS, Yamamoto BM, Riffell JA, Imaizumi T. 2015. Circadian clock gene *LATE ELONGATED HYPOCOTYL* directly regulates the timing of floral scent emission in *Petunia*. *Proceedings of the National Academy of Sciences, USA* **112**: 9775–9780.

Fernandez-Pozo N, Rosli HG, Martin GB, Mueller LA. 2015. The SGN VIGS tool: user-friendly software to design virus-induced gene silencing (VIGS) Constructs for functional genomics. *Molecular Plant* **8**: 486–488.

Frick S, Kutchan TM. 1999. Molecular cloning and functional expression of O-methyltransferases common to isoquinoline alkaloid and phenylpropanoid biosynthesis. *The Plant Journal* **17**: 329–339.

Fujii T, Matsuda S, Tejedor ML, Esaki T, Sakane I, Mizuno H, Tsuyama N, Masujima T. 2015. Direct metabolomics for plant cells by live single-cell mass spectrometry. *Nature Protocols* **10**: 1445–1456.

Guo H, Lackus ND, Köllner TG, Li R, Bing J, Wang Y, Baldwin IT, Xu S. 2020. Evolution of a novel and adaptive floral scent in wild tobacco. *Molecular Biology and Evolution* **37**: 1090–1099.

Guterman I, Shalit M, Menda N, Piestun D, Dafny-Yelin M, Shalev G, Bar E, Davydov O, Ovadis M, Emanuel M *et al.* 2002. Rose scent: genomics approach to discovering novel floral fragrance-related genes. *Plant Cell* **14**: 2325–2338.

Hafemeister C, Satija R. 2019. Normalization and variance stabilization of single-cell RNA-seq data using regularized negative binomial regression. *Genome Biology* **20**: 1–15.

Haverkamp A, Yon F, Keesey IW, Mißbach C, Koenig C, Hansson BS, Baldwin IT, Knaden M, Kessler D. 2016. Hawkmoths evaluate scenting flowers with the tip of their proboscis. *eLife* **5**: 1–12.

Jean-Baptiste K, McFaline-Figueroa JL, Alexandre CM, Dorrity MW, Saunders L, Bubb KL, Trapnell C, Fields S, Queitsch C, Cuperusa JT. 2019. Dynamics of gene expression in single root cells of *Arabidopsis thaliana*. *Plant Cell* **31**: 993–1011.

Joo Y, Schuman MC, Goldberg JK, Wissgott A, Kim SG, Baldwin IT. 2019. Herbivory elicits changes in green leaf volatile production via jasmonate signaling and the circadian clock. *Plant, Cell & Environment* **42**: 972–982.

Kallenbach M, Oh Y, Eilers EJ, Veit D, Baldwin IT, Schuman MC. 2014. A robust, simple, high-throughput technique for time-resolved plant volatile analysis in field experiments. *The Plant Journal* **78**: 1060–1072.

Kang M, Ahn H, Rothe E, Baldwin IT, Kim SG. 2020. A robust genome-editing method for wild plant species *Nicotiana attenuata*. *Plant Biotechnology Reports* **14**: 585–598.

Karimi M, Inzé D, Depicker A. 2002. GATEWAY vectors for *Agrobacterium*-mediated plant. *Trends in Plant Science* **7**: 193–195.

Kessler D, Baldwin IT. 2007. Making sense of nectar scents: the effects of nectar secondary metabolites on floral visitors of *Nicotiana attenuata*. *The Plant Journal* **49**: 840–854.

Kessler D, Bing J, Haverkamp A, Baldwin IT. 2019. The defensive function of a pollinator-attracting floral volatile. *Functional Ecology* **33**: 1223–1232.

Kessler D, Gase K, Baldwin IT. 2008. Field experiments with transformed plants reveal the sense of floral scents. *Science* **321**: 1200–1202.

Kim J-Y, Symeonidi E, Pang TY, Denyer T, Weidauer D, Bezrutczyk M, Miras M, Zöllner N, Hartwig T, Wudick MM *et al.* 2021. Distinct identities of leaf phloem cells revealed by single cell transcriptomics. *Plant Cell* **33**: 511–530.

Kim SG, Yon F, Gaquerel E, Gulati J, Baldwin IT. 2011. Tissue specific diurnal rhythms of metabolites and their regulation during herbivore attack in a native tobacco, *Nicotiana attenuata*. *PLoS ONE* **6**: e26214.

Klempien A, Kaminaga Y, Qualley A, Nagegowda DA, Widhalm JR, Orlova I, Shasany AK, Taguchi G, Kish CM, Cooper BR *et al.* 2012. Contribution of CoA ligases to benzenoid biosynthesis in petunia flowers. *Plant Cell* **24**: 2015–2030.

Knudsen JT, Eriksson R, Gershenzon J, Ståhl B. 2006. Diversity and distribution of floral scent. *Botanical Review* **72**: 1–120.

Knudsen JT, Gershenzon J. 2020. The chemical diversity of floral scent. In: Pichersky E, Dudareva N, eds. *Biology of plant volatiles*. Boca Raton, FL, USA: CRC Press, 22.

Koeduka T, Watanabe B, Suzuki S, Hiratake J, Mano J, Yazaki K. 2011. Characterization of raspberry ketone/zingerone synthase, catalyzing the alpha, beta-hydrogenation of phenylbutenones in raspberry fruits. *Biochemical and Biophysical Research Communications* **412**: 104–108.

Kolosova N, Sherman D, Karlson D, Dudareva N. 2001. Cellular and subcellular localization of S-adenosyl-L-methionine : benzoic acid carboxyl methyltransferase, the enzyme responsible for biosynthesis of the volatile ester methylbenzoate in snapdragon flowers. *Plant Physiology* **126**: 956–964.

Krassowski M. 2020. *COMPLEXUPSET*. doi: 10.5281/zenodo.3700590.

Krügel T, Lim M, Gase K, Halitschke R, Baldwin IT. 2002. *Agrobacterium*-mediated transformation of *Nicotiana attenuata*, a model ecological expression system. *Chemoecology* **12**: 177–183.

Langdale JA, Nelson T. 1991. Spatial regulation of photosynthetic development in C_4 plants. *Trends in Genetics* **7**: 191–196.

Lee D, Meyer K, Chapple C, Douglas CJ. 1997. Antisense suppression of 4-coumarate : coenzyme A ligase activity in *Arabidopsis* leads to altered lignin subunit composition. *Plant Cell* **9**: 1985–1998.

Lex A, Gehlenborg N, Strobelt H, Vuillemot R, Pfister H. 2014. UpSet: visualization of intersecting sets. *IEEE Transactions on Visualization and Computer Graphics* **20**: 1983–1992.

Li D, Heiling S, Baldwin IT, Gaquerel E. 2016. Illuminating a plant's tissue-specific metabolic diversity using computational metabolomics and information theory. *Proceedings of the National Academy of Sciences, USA* **113**: E7610–E7618.

Li Z, Wang Z, Wang K, Liu Y, Hong Y, Chen C, Guan X, Chen Q. 2020. Co-expression network analysis uncovers key candidate genes related to the regulation of volatile esters accumulation in Woodland strawberry. *Planta* **252**: 1–15.

Libault M, Pingault L, Zogli P, Schiefelbein J. 2017. Plant systems biology at the single-cell level. *Trends in Plant Science* **22**: 949–960.

Lopez-anido CB, Vatén A, Smoot NK, Sharma N, Guo V, Gong Y, Gil XA, Weimer AK, Bergmann DC. 2020. Single-cell resolution of lineage trajectories in the *Arabidopsis* stomatal lineage and developing leaf. *Developmental Cell* **56**: 1043–1055.e4.

Magnard JL, Roccia A, Caissard JC, Vergne P, Sun P, Hecquet R, Dubois A, Saint OLH, Jullien F, Nicolè F *et al.* 2015. Biosynthesis of monoterpene scent compounds in roses. *Science* **349**: 81–83.

Maruyama-Nakashita A, Watanabe-Takahashi A, Inoue E, Yamaya T, Saito K, Takahashi H. 2015. Sulfur-responsive elements in the 3′-nontranscribed intergenic region are essential for the induction of *SULFATE TRANSPORTER 2;1* gene expression in *Arabidopsis* roots under sulfur deficiency. *Plant Cell* **27**: 1279–1296.

Misra BB, Assmann SM, Chen S. 2014. Plant single-cell and single-cell-type metabolomics. *Trends in Plant Science* **19**: 637–646.

Morita H, Shimokawa Y, Tanio M, Kato R, Noguchi H, Sugio S, Kohno T, Abe I. 2010. A structure-based mechanism for benzalacetone synthase from *Rheum palmatum*. *Proceedings of the National Academy of Sciences, USA* **107**: 669–673.

Muhlemann JK, Klempien A, Dudareva N. 2014. Floral volatiles: from biosynthesis to function. *Plant, Cell & Environment* **37**: 1936–1949.

Qualley AV, Widhalm JR, Adebesin F, Kish CM, Dudareva N. 2012. Completion of the core β-oxidative pathway of benzoic acid biosynthesis in

plants. *Proceedings of the National Academy of Sciences, USA* **109**: 16383–16388.

Ryu KH, Huang L, Kang HM, Schiefelbein J. 2019. Single-cell RNA sequencing resolves molecular relationships among individual plant cells. *Plant Physiology* **179**: 1444–1456.

Saedler R, Baldwin IT. 2004. Virus-induced gene silencing of jasmonate-induced direct defences, nicotine and trypsin proteinase-inhibitors in *Nicotiana attenuata*. *Journal of Experimental Botany* **55**: 151–157.

Satija R, Farrell JA, Gennert D, Schier AF, Regev A. 2015. Spatial reconstruction of single-cell gene expression data. *Nature Biotechnology* **33**: 495–502.

Satterlee JW, Strable J, Scanlon MJ. 2020. Plant stem-cell organization and differentiation at single-cell resolution. *Proceedings of the National Academy of Sciences, USA* **117**: 33689–33699.

Scalliet G, Lionnet C, Le BM, Dutron L, Magnard J-L, Baudino S, Bergougnoux V, Jullien F, Chambrier P, Vergne P *et al.* 2006. Role of petal-specific orcinol O-methyltransferases in the evolution of rose scent. *Plant Physiology* **140**: 18–29.

Schmittgen TD, Livak KJ. 2008. Analyzing real-time PCR data by the comparative C_T method. *Nature Protocols* **3**: 1101.

Shimokawa Y, Morita H, Abe I. 2012. Benzalacetone synthase. *Frontiers in Plant Science* **3**: 1–6.

Shinozaki Y, Nicolas P, Fernandez-Pozo N, Ma Q, Evanich DJ, Shi Y, Xu Y, Zheng Y, Snyder SI, Martin LBB *et al.* 2018. High-resolution spatiotemporal transcriptome mapping of tomato fruit development and ripening. *Nature Communications* **9**: 1–13.

Shulse CN, Cole BJ, Ciobanu D, Lin J, Yoshinaga Y, Gouran M, Turco GM, Zhu Y, O'Malley RC, Brady SM *et al.* 2019. High-throughput single-cell transcriptome profiling of plant cell types. *Cell Reports* **27**: 2241–2247.e4.

Spitzer-Rimon B, Farhi M, Albo B, Cna'ani A, Ben Zvi MM, Masci T, Edelbaum O, Yu Y, Shklarman E, Ovadis M *et al.* 2013. The R2R3-MYB-like regulatory factor EOBI, acting downstream of EOBII, regulates scent production by activating *ODO1* and structural scent-related genes in petunia. *Plant Cell* **24**: 5089–5105.

Spitzer-Rimon B, Marhevka E, Barkai O, Marton I, Edelbaum O, Masci T, Prathapani NK, Shklarman E, Ovadis M, Vainstein A. 2010. *EOBII*, a gene encoding a flower-specific regulator of phenylpropanoid volatiles' biosynthesis in petunia. *Plant Cell* **22**: 1961–1976.

Stockhaus J, Schlue U, Koczor M, Chitty JA, Taylor WC, Westhoff P. 1997. The promoter of the gene encoding the C_4 form of phosphoenolpyruvate carboxylase directs mesophyll-specific expression in transgenic C_4 *Flaveria* spp. *Plant Cell* **9**: 479–489.

Suh MC, Samuels AL, Jetter R, Kunst L, Pollard M, Ohlrogge J, Beisson F. 2005. Cuticular lipid composition, surface structure, and gene expression in *Arabidopsis* stem epidermis. *Plant Physiology* **139**: 1649–1665.

Van Moerkercke A, Haring MA, Schuurink RC. 2011. The transcription factor EMISSION of BENZENOIDS II activates the MYB *ODORANT1* promoter at a MYB binding site specific for fragrant petunias. *The Plant Journal* **67**: 917–928.

Verdonk JC, Haring MA, Van Tunen AJ, Schuurink RC. 2005. *ODORANT1* regulates fragrance biosynthesis in petunia flowers. *Plant Cell* **17**: 1612–1624.

Wang X, He X, Lin J, Shao H, Chang Z, Dixon RA. 2006. Crystal structure of isoflavone reductase from Alfalfa (*Medicago sativa* L.). *Journal of Molecular Biology* **358**: 1341–1352.

Widhalm JR, Dudareva N. 2015. A familiar ring to it: biosynthesis of plant benzoic acids. *Molecular Plant* **8**: 83–97.

Wisecaver JH, Borowsky AT, Tzin V, Jander G, Kliebenstein DJ, Rokas A. 2017. A global coexpression network approach for connecting genes to specialized metabolic pathways in plants. *Plant Cell* **29**: 944–959.

Wong DCJ, Peakall R, Pichersky E. 2020. The role of transcriptome analysis in shaping the discovery of plant volatile genes. In: Pichersky E, Dudareva N, eds. *Biology of plant volatiles*. Boca Raton, FL, USA: CRC Press.

Wu H, Kirita Y, Donnelly EL, Humphreys BD. 2019. Advantages of single-nucleus over single-cell RNA sequencing of adult kidney: rare cell types and novel cell states revealed in fibrosis. *Journal of the American Society of Nephrology* **30**: 23–32.

Wypych G. 2015. 3 – Mechanisms of UV stabilization. In: Wypych G, ed. *Handbook of UV degradation and stabilization, 2nd edn*. Toronto, ON, Canada: ChemTec Publishing, 37–65.

Xu H, Moghe GD, Wiegert-Rininger K, Schilmiller AL, Barry CS, Last RL, Pichersky E. 2018. Coexpression analysis identifies two oxidoreductases involved in the biosynthesis of the monoterpene acid moiety of natural pyrethrin insecticides in *Tanacetum cinerariifolium*. *Plant Physiology* **176**: 524–537.

Yon F, Joo Y, Cortés Llorca L, Rothe E, Baldwin IT, Kim SG. 2016. Silencing *Nicotiana attenuata LHY* and *ZTL* alters circadian rhythms in flowers. *New Phytologist* **209**: 1058–1066.

Yoo SD, Cho YH, Sheen J. 2007. *Arabidopsis* mesophyll protoplasts: a versatile cell system for transient gene expression analysis. *Nature Protocols* **2**: 1565–1572.

Zhang T, Chen Y, Wang J, Zhang T, Chen Y, Wang J. 2021. A single-cell analysis of the *Arabidopsis* vegetative shoot apex. *Developmental Cell* **56**: 1–19.

Supporting Information

Additional Supporting Information may be found online in the Supporting Information section at the end of the article.

Fig. S1 Correlation analysis between bulk-RNA-Seq and scRNA-Seq datasets.

Fig. S2 QC metrics of scRNA-Seq datasets.

Fig. S3. Cells are displayed by an integrated uniform manifold approximation and projection (UMAP) plot in two dimensions.

Fig. S4 Pollen and vasculature-specific marker genes are exclusively expressed in clusters 7 and 8, respectively.

Fig. S5 Validation of pollen-specific marker genes.

Fig. S6 Putative wax and cutin biosynthesis genes are more expressed in clusters 0, 3, 4, 5, and 9.

Fig. S7 Protein sequences of marker genes are similar to their *Arabidopsis thaliana* orthologs.

Fig. S8 Subunits of photosystems I and II complexes are enriched in clusters 1, 2, and 6.

Fig. S9 NaPKS1/2/3/4 share high sequence similarity with polyketide synthase proteins of other species.

Fig. S10 Target sequences for NaPKS RNAi experiments (used in previous studies, NaCHAL) and VIGS experiments (used in this study).

Fig. S11 Cladogram of *Nicotiana attenuata* 4CL, CNL homologs within acyl-activating enzyme (AAE) superfamily.

Fig. S12 4CL and CNL homologs are not co-silenced in *Na4CL1*-silenced flowers.

Fig. S13 Co-silencing of *NaPKS1/2/3/4* in *NaPKS3*-VIGS flowers.

Fig. S14 Tissue-specific expression of *NaPKS2* and *NaPKS3* in *Nicotiana attenuata*.

Fig. S15 AER homologs are not co-silenced in *NaAER1*-silenced flowers.

Fig. S16 Extinction coefficients used for NaAER1 kinetics.

Fig. S17 NaAER1 can reduce benzalacetone to benzylacetone.

Fig. S18 Silencing *NaIFR* transcription does not alter BA biosynthesis in corolla.

Fig. S19 *NaPAL4* transcripts are highly expressed in clusters 0, 3, and 4.

Fig. S20 Expression of *NaPAL4* and *NaPKS2* in *Nicotiana attenuata* flowers.

Fig. S21 *Nicotiana attenuata* homologs of *Petunia*×*hybrida* MYB transcription factors.

Fig. S22 *NaIFR3* expression patterns in scRNA-Seq dataset.

Table S1 One hundred and twenty-one genes excluded for analysis.

Table S2 Primers used in this study.

Please note: Wiley Blackwell are not responsible for the content or functionality of any Supporting Information supplied by the authors. Any queries (other than missing material) should be directed to the *New Phytologist* Central Office.